

MPM-402781 (Revision 1)

**Benchmarking  
of  
Nine Mile Point  
Unit 1 and Unit 2  
Neutron  
Transport  
Calculations**



*...serving client needs  
through advanced technology...*

© Copyright 2003 MPM Technologies, Inc.  
All Rights Reserved

**September, 2003**

## Copyright Notice

The publication listed below bears a 2003 Copyright Notice. MPM Technologies, Inc., holder of the copyright, hereby grants the Nuclear Regulatory Commission (NRC) the authority to make the number of copies of this copyrighted material which are necessary for its internal use and to fulfill its legal responsibilities as regards public disclosure. This authorization is granted with the understanding that any copies of the publication made by the NRC will continue to bear the following copyright notice, which will be reproduced along with any portion of the publication:

The report listed below contains material copyrighted by MPM Technologies, Inc. Material reproduced by permission of MPM Technologies, Inc.

“Benchmarking of Nine Mile Point Unit 1 and Unit 2 Neutron Transport Calculations”,  
Report MPM-402781 (Revision 1), MPM Technologies, Inc., 2161 Sandy Drive, State  
College, PA 16803-2283, September, 2003.

MPM Technologies, Inc.

*M. P. Manahan, Sr.*

---

M. P. Manahan, Sr.  
President

**Final Report**

*entitled*

**Benchmarking of Nine Mile Point Unit 1 and Unit 2  
Neutron Transport Calculations**

*prepared for*

**Constellation Generation Group  
Nine Mile Point Units 1 and 2  
Lake Road  
Lycoming, NY 13093**

*by*

**MPM Technologies, Inc.  
2161 Sandy Drive  
State College, PA 16803-2283**

**September, 2003**



---

**Preparer  
8/7/03**

---

**Date**

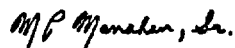


---

**Checker  
9/3/03**

---

**Date**



---

**MPM Approval**

**9/3/03**

---

**Date**

## Nuclear Quality Assurance Certification

---

This document certifies that MPM has performed all work under Nine Mile Point Station Purchase Order Number 01-35807-003 in accordance with the requirements of the Purchase Order. All work has been performed under the MPM Nuclear Quality Assurance Program.

*M. P. Manahan, Sr.*

---

**M. P. Manahan, Sr.**  
**President**  
**9/3/03**

---

**Date**

*Richard P. Erhard*

---

**R. Erhard**  
**QA Manager**  
**9/3/03**

---

**Date**

## **Revision 1 Summary of Technical Changes**

Detailed data on the breakdown of fission by isotope was not available at the time previous calculations were performed for NMP-1 and NMP-2. To overcome this deficiency, the ORIGEN (version 2.1) computer code was used to calculate the fission distribution by isotope as a function of fuel burnup for determination of the fission source. An Appendix has been added to provide validation of the application of the Origen code for determination of fission source by isotope for NMP.

In the previous analysis of the PCA, some difficulty was encountered with the Rh103 and U238 dosimetry comparisons. Revisions to the Section 3.0 have been made which document the analyses performed to resolve previous difficulties. Section 3.0 also provides a discussion on the validity of the PCA as a BWR benchmark.

The NRC has requested that all of the NMP-1 surveillance capsule dosimetry data be analyzed and reported. Revised Section 5 provides the requested analyses and includes new and/or updated C/M ratios for all vessel surveillance capsule dosimeters and for the NMP-1 core shroud boat sample measurements. Section 5 has also been updated to reflect the upgraded NMP-1 plant model and added fuel cycle analyses.

The Section 6 summary and conclusions and Section 7 references have been revised to incorporate the results of the Section 3 and 5 changes.

Minor editorial and typographical changes have been made throughout the report. These corrections have not resulted in any substantive technical changes.

## **Executive Summary**

---

In March 2001, the Nuclear Regulatory Commission (NRC) issued Regulatory Guide (RG) 1.190, "Calculational and Dosimetry Methods for Determining Pressure Vessel Neutron Fluence." Although specifically developed to address calculation of fluence to the vessel, the guide can be considered to apply to other reactor components such as the shroud or surveillance capsule. One of the requirements of RG 1.190 is the benchmarking of the methodology used in the fluence determination. This report documents calculations performed to qualify the MPM methodology as applied for fluence determination for Nine Mile Point Unit 1 and Unit 2.

In order to meet the methods qualification requirement of RG 1.190, the MPM calculational methodology has been validated by comparison with measurement and calculational benchmarks. Comparisons of calculations with measurements have been made in the Pool Critical Assembly (PCA) pressure vessel simulator benchmark and in the Nine Mile Point Units 1 and 2 (NMP-1 and NMP-2) operating plants. Comparisons with a BWR calculational benchmark have also been completed.

The PCA has high-accuracy measurement results extending from inside a simulated thermal shield through to the outside of a simulated vessel. Measurements were made with this simulator arranged in a variety of geometries, including in some cases simulated surveillance capsules, but the recommended benchmark consists of a single geometry which includes a 12 cm gap between the reactor core and thermal shield plate, and a 13 cm gap between the thermal shield and the vessel simulator. While this geometry is more typical of PWR geometries than that of BWRs, these are the largest water gaps studied in the PCA. It is felt that this PCA geometry comes the closest to operating BWR geometries of any recommended experimental benchmarks, and thus is the most applicable for benchmark testing of BWR calculations as applied to the reactor vessel and in-vessel structures. The calculational results in the PCA show a slight consistent bias (averaging 6%) with respect to the measurements, but no significant change in bias is observed with change in irradiation position. This indicates that the transport methodology is calculating the flux attenuation outside the core region with high accuracy. The observed bias is consistent with that obtained by other synthesis calculations.

The calculational benchmark was a typical BWR geometry similar to those of NMP-1 and NMP-2. Comparisons were made between the MPM calculations and the benchmark calculational results which indicated very good agreement. In the capsule the average results were about 3% low, and at the vessel inner radius (IR) and within the vessel, the average results were about 2-3% high. All compared results fell within  $\pm 10\%$ .

Comparisons were made with surveillance capsule measurements in NMP-1 and NMP-2 and with shroud measurements in NMP-1. For the four sets of NMP-1 capsule dosimetry, all of the calculated dosimeter activities fall well within  $\pm 20\%$  of the measurement. Moreover, if the four sets are averaged, the average calculated-to-measured (C/M) ratio is very close to 1.0. Similar consistency is obtained for the NMP-2 capsule. In all the capsule cases, agreement with

measured results within uncertainty was obtained and uncertainties were shown to be less than  $\pm 20\%$ . This meets the criterion set by RG 1.190 for acceptability of the calculations.

For the NMP-1 shroud boat sample measurements, calculated results all fell within  $\pm 20\%$  of the measurement except for the Ni reaction at the lower weld location, which gave a C/M ratio of 1.23. The cause for the lower core shroud location (V10) boat sample Ni C/M ratio being 1.23 is well understood. Review of the boat sample data has led to the conclusion that the end-of-cycle power shift toward the top of the core is significant in cycle 12 and causes a decrease in the flux below core mid-plane during the final 6 months of the cycle. This shift is not captured by the 5 case breakdown used to model the average cycle 12 flux calculation. Because of the short half-life, Ni is very sensitive to these end-of-cycle power shift effects. These effects are not significant relative to predicting the cycle average flux as is demonstrated by the good agreement for the Fe dosimeter for the same location. While it is possible to resolve the Ni dosimeter data with further detailed end-of-cycle 12 analysis, this effort is not considered warranted to qualify the methods or to define the cycle average flux. Therefore, the Ni reaction at shroud weld V10 has been disqualified and the Ni boat sample data have been excluded from the overall C/M ratio calculation for the V10 location. The conclusions reached in previous reports with regard to the boat sample comparisons remain unchanged. Accordingly, the overall C/M ratio for the boat samples has been shown to be less than  $\pm 20\%$  and the Ni reaction at V10 is not needed to determine the cycle average flux nor to qualify the NMP plant-specific fluence calculational methodology.

In summary, it is concluded that the RG 1.190 requirement for qualification of the MPM methodology used for NMP-1 and NMP-2 by comparisons to measurement and calculational benchmarks has been fully satisfied. Moreover, the agreement of calculations with measurements in the NMP-1 and NMP-2 plants within uncertainty indicates that the calculations can be applied for fluence determination with no bias.

# Contents

---

Executive Summary .....	Preface Page iii
1.0 Introduction .....	Page Number 1
2.0 Neutron Flux Computational Method .....	Page Number 3
2.1 Neutron Transport Model .....	Page Number 3
2.2 Compliance with RG 1.190 .....	Page Number 4
3.0 PCA Benchmark Calculation .....	Page Number 10
4.0 BWR Computational Benchmark .....	Page Number 20
5.0 Plant-specific Benchmarking .....	Page Number 28
5.1 NMP-1 Benchmarks .....	Page Number 28
5.2 NMP-2 Benchmark .....	Page Number 34
5.3 Summary of Plant-Specific Benchmark Results .....	Page Number 38
6.0 Summary and Conclusions .....	Page Number 47
7.0 Nomenclature .....	Page Number 48
8.0 References .....	Page Number 49
Appendix .....	Page Number 53

## 1.0 Introduction

---

In March 2001, the Nuclear Regulatory Commission (NRC) issued Regulatory Guide (RG) 1.190, "Calculational and Dosimetry Methods for Determining Pressure Vessel Neutron Fluence" [1]. This guide is the final version of two previous draft guides, DG-1053 and DG-1025. The guide was developed to provide state-of-the-art calculational and measurement procedures that are acceptable to the NRC staff for determining pressure vessel fluence. Although specifically developed to address calculation of fluence to the vessel, the guide can be considered to apply to other reactor components such as the shroud and the surveillance capsules.

One of the requirements of RG 1.190 is the benchmarking of the methodology used in the fluence determination. Specifically, RG 1.190 has the following requirement:

*Methods Qualification. The calculational methodology must be qualified by both (1) comparisons to measurement and calculational benchmarks and (2) an analytic uncertainty analysis. The methods used to calculate the benchmarks must be consistent (to the extent possible) with the methods used to calculate the vessel fluence. The overall calculational bias and uncertainty must be determined by an appropriate combination of the analytic uncertainty analysis and the uncertainty analysis based on the comparisons to the benchmarks.*

Fluences in various reactor components for Nine Mile Point Units 1 and 2 (NMP-1 and NMP- 2) have been evaluated in several reports [2, 3, 4] prepared prior to the issuance of RG 1.190 in March, 2001. In addition, an update of the NMP-2 shroud fluence evaluation has been issued [5, 6]. The fluence analyses in these reports were fully compliant with RG 1.190 except for part of the benchmarking requirement for methods qualification. This report completes that requirement and, thereby, makes all the analyses totally consistent with RG 1.190.

Benchmarking the methodology requires more than one analysis. Because fluence measurements cannot be made at all of the actual points of interest in an operating plant, neutron transport calculations are necessary to obtain the fluence at all important locations. Since the calculations involve many parameters, agreement of calculations with measurements at one point in space cannot guarantee the same calculational accuracy at other points. This report contains documentation of several benchmark analyses pertinent to BWR calculations. Taken together, they provide a validation of the calculational method for accurate determination of the fluence at all regions between the core and the outside of the reactor vessel.

The first benchmark is a calculation of the Pool Critical Assembly (PCA) simulated reactor vessel [7]. This benchmark provides validation of the transport through typical reactor structures and the simulated reactor vessel in a simple geometry. It provides a test of the transport methodology in a reactor geometry and enables a comparison of the calculational results within the vessel structure with measurements. While the PCA geometry is more typical of PWR geometries than that of BWRs it is felt that the PCA geometry with the largest water

gaps comes the closest of any recommended benchmark to replicating BWR conditions, and thus is the most applicable for benchmark testing of BWR calculations as applied to the reactor vessel and to in-vessel structures.

The second benchmark is a calculational benchmark for a typical BWR geometry [8]. While this benchmark does not provide verification of the methodology by comparison with measurements, it does enable a check for the consistency of the methodology with results calculated by NRC contractors using standard techniques. Agreement with this benchmark ensures that the transport results obtained for BWR plants include all important factors for accurate transport in BWR geometries. BWR analyses involve more complex modeling situations than encountered in PWR plant analyses due to such factors as asymmetric geometry, fuel burnup, and fuel region void fractions.

The third set of benchmarks is a comparison with dosimetry measurements in actual BWR plants. While the other benchmarks provide validation of the methodology, only comparisons with actual plant measurements can verify that the correct plant information has been included in the analysis. Plant-specific comparisons enable biases to be identified that arise from uncertainties in the plant dimensions, power distributions, operating conditions, etc.

Successful completion of the analyses described above, as indicated by agreement with measurements or other calculations within tolerance, completely satisfies the methodology qualification requirement. In addition, application of the methodology to a specific plant requires an analytic uncertainty analysis for each plant-specific case. These uncertainty analyses are included in the report prepared for each specific plant.

## 2.0 Neutron Flux Computational Method

---

### 2.1 Neutron Transport Model

The neutron exposure of reactor structures is determined by a neutron transport calculation, or a combination of neutron transport calculations, to represent the distribution of neutron flux in three dimensions. The calculation determines the distribution of neutrons of all energies from their source from fission in the core region to their eventual absorption or leakage from the system. The calculation uses a model of the reactor geometry that includes the significant structures and geometrical details necessary to define the neutron environment at locations of interest.

The transport calculations reported here were carried out using the DORT two-dimensional discrete ordinates code [9] and the BUGLE-96 cross-section library [10]. Other codes used for DORT input preparations included the DOTSOR code (available as part of the LEPRICON code package [11]), which was used to convert core power distributions from X,Y to R, $\theta$  coordinates and place the source in each mesh cell, and the ORIGEN 2.1 code [12], which was used to calculate the effects of burnup on the neutron source. Since ORIGEN has not been commonly used for this purpose, the difference between transport results using a neutron source based on ORIGEN calculations and on fuel burnup codes is discussed in the appendix to this report and shown to be small. Results from the DORT transport calculations were synthesized using the DOTSYN code (also available as part of the LEPRICON code package [11]). The computer codes and data libraries were obtained from the Radiation Safety Information Computational Center (RSICC) at Oak Ridge National Laboratory (ORNL). Each code was then compiled on the computer used by MPM for the calculations and a series of test cases were run to verify the code performance. The test cases all agreed within allowable tolerance with established results. This verification was conducted under the MPM Nuclear Quality Assurance Program.

The DORT code is an update of the DOT code which has been in use for this type of problem for many years. It is routinely used and has been used by others for benchmarking calculations [7, 8, 13, 14]. In the analyses, anisotropic scattering was treated with a  $P_3$  expansion of the scattering cross-sections, and the angular discretization was modeled with an  $S_8$  order of angular quadrature. These procedures are in accordance with RG 1.190 and ASTM Standard E-482 [15].

The BUGLE-96 library is a 47 energy group ENDF/B-VI based data set produced specifically for light water reactor shielding and pressure vessel dosimetry applications (an update of the earlier SAILOR library). The energy group boundaries for the 47 groups are given in Table 2-1. This library contains cross-sections collapsed using flux spectra from both BWR and PWR reactor models. Within the core region, cross section sets are collapsed using a PWR core spectrum and a BWR core spectrum. Outside the core, cross sections are produced using a PWR downcomer spectrum, a PWR vessel 1/4 T spectrum, and a concrete spectrum. References

[16, 17] detail the data testing of the BUGLE libraries and validation of their applicability for LWR shielding calculations.

As indicated above, the DORT code calculates the neutron transport in two dimensions. In order to estimate the fluence rate in the three-dimensional geometry, the following equation was used to synthesize the flux  $\phi$  for each case of cylindrical geometry:

$$\phi(R, \theta, Z) = \phi(R, \theta) * \phi(R, Z) / \phi(R)$$

In this equation,  $\phi(R, \theta)$  is taken from the DORT R,  $\theta$  calculation (normalized to the power at midplane in the model region), and  $\phi(R, Z)$  is from the R, Z calculation normalized to the power in the entire core. A third calculation determined  $\phi(R)$  using a one-dimensional cylindrical model normalized at core midplane. The one-dimensional calculation uses the same radial geometry and source distribution as the R, Z calculation at core midplane. In the case of the PCA benchmark, the calculation was carried out in X, Y, Z geometry and a similar synthesis equation was used.

For each calculation, a detailed model of the reactor geometry was developed. The models contain all of the significant reactor structures and use a mesh structure that is fine enough to give good flux convergence. Typically, the radial mesh will be the most critical because of the large flux attenuation of neutrons as they are transported from the core to the vessel region. Most radial mesh intervals outside the core are smaller than 1 cm. This is particularly important in steel structures for calculation of the flux above 1 MeV. Models of large reactor geometries, such as for BWRs, will have 140 to 200 radial mesh points. In the azimuthal direction models have 40 to 80 mesh points to cover an octant of the reactor, depending on the structures to be defined. In the axial direction, models may have as many as 150 mesh points, or more. Modeling smaller reactor geometries, such as the PCA, do not require as many points.

## 2.2 Compliance with RG 1.190

Regulatory Guide 1.190 covers recommended practices for neutron transport calculations and applies to other reactor components in addition to the primary emphasis on the pressure vessel. The regulatory positions in the guide that pertain to calculational methodology are summarized in Table 2-2 which is taken directly from the guide. The table references paragraphs in the guide that give more detailed information on each position. The compliance of the MPM calculational methodology with the guide is summarized below.

*Fluence Determination:* All calculations were performed using an absolute fluence calculation. Meets guide requirement.

*Modeling Data:* All the data used in the models are documented and verified. Meets guide requirement.

***Nuclear Data:*** The calculations use the BUGLE-96 cross section set which is based on the latest version (VI) of the Evaluated Nuclear Data File (ENDF/B). The BUGLE-96 set has undergone extensive testing and benchmarking to ensure its validity for LWR calculations. Meets guide requirement.

***Cross-Section Angular Representation:*** The calculations use a P3 angular expansion in accordance with the guide. Meets guide requirement.

***Cross-Section Group Collapsing:*** The calculations use the BUGLE-96 library without additional collapsing. Benchmarking has shown that the 47 group structure is adequate for LWR neutron transport calculations. Meets guide requirement.

***Neutron Source:*** Isotopic variation is accounted for in the neutron spectrum, neutrons per fission, and energy per fission within the modeling limitations. Moderator density is included in detail. Meets guide requirement.

***End-of-Life Predictions:*** No fluence projections are made in this benchmarking effort. Fluence projections for plant analyses use best-estimate fuel loadings. Meets guide requirement.

***Spatial Representation:*** Mesh intervals are adopted to ensure that flux changes within intervals are small enough to allow for accurate results. Radial intervals in the outer core region and in the region between the core and the outside of the vessel are generally about 1 cm except near boundaries where a finer mesh is used in some cases. Inside the core, where flux changes are small, larger intervals are used. In the azimuthal direction, between 40 and 80 meshes are used, depending on the complexity of structures to be modeled. In the axial direction, a coarse mesh is acceptable in regions where the flux changes slowly. Finer meshing is used near boundaries. The quadrature used was S8. Meets guide requirement.

***Multiple Transport Calculations:*** It was not necessary to use bootstrapping for these calculations so this requirement does not apply.

***Point Estimates:*** This requirement only applies to Monte Carlo calculations which are not used here.

***Statistical Tests:*** This requirement only applies to Monte Carlo calculations which are not used here.

***Variance Reduction:*** This requirement only applies to Monte Carlo calculations which are not used here.

***Spectral Effects on  $RT_{NDT}$ :*** This requirement only applies to extrapolation through the vessel and does not affect the benchmark calculations. However, when fluence within the vessel is required, the displacement per atom (dpa) methodology is applied to vessel calculations as specified in RG 1.99, Revision 2 [18] (see, for example, Reference [3]).

Meets guide requirement.

***Cavity Calculations:*** With the exception of the one dosimetry measurement at the rear of the PCA vessel, no cavity results have been applied for this benchmarking effort. In the event that cavity dosimetry measurements are analyzed in the future, it will be necessary to ensure that the quadrature is adequate. Utilization of cavity flux calculations is not anticipated at this time.

Meets guide requirement.

***Methods Qualification:*** These calculations and comparisons provide the required methods qualification. This includes verification of vessel fluence calculations using the PCA simulator measurements, the BWR calculational benchmark, and comparisons with plant-specific BWR measurements. No uncertainty analysis was performed for the PCA calculation or for the BWR calculational benchmark since no uncertainty data is given with these problems. Comparisons with measurements or with standard results provide validation of the accuracy of the calculations. A complete analytical uncertainty analysis was carried out in accordance with the guide for the NMP-1 and NMP-2 calculations. This uncertainty analysis indicated that calculational errors for vessel fluences in the beltline region were about 15%, well within the 20% accuracy requirement specified by RG 1.190.

Meets guide requirement.

***Fluence Calculational Uncertainty:*** An extensive evaluation of all contributors to the uncertainty in the calculated fluence was made for the NMP-1 and NMP-2 calculations. This evaluation indicated that the uncertainty in calculated fluences in the reactor beltline region is below 20% as specified in the guide. In addition, the comparisons with measurements indicate agreement well within the 20% limit. Thus, fluence evaluations using the present methodology applied to NMP-1 and NMP-2 will use the calculated results with no bias applied.

Meets guide requirement.

**Table 2-1 Neutron Energy Group Structure – 47 Groups.**

Energy Group	Upper Energy (MeV)	Energy Group	Upper Energy (MeV)
1	1.733E+01	25	2.972E-01
2	1.419E+01	26	1.832E-01
3	1.221E+01	27	1.111E-01
4	1.000E+01	28	6.738E-02
5	8.607E+00	29	4.087E-02
6	7.408E+00	30	3.183E-02
7	6.065E+00	31	2.606E-02
8	4.966E+00	32	2.418E-02
9	3.679E+00	33	2.188E-02
10	3.012E+00	34	1.503E-02
11	2.725E+00	35	7.102E-03
12	2.466E+00	36	3.355E-03
13	2.365E+00	37	1.585E-03
14	2.346E+00	38	4.540E-04
15	2.231E+00	39	2.145E-04
16	1.920E+00	40	1.013E-04
17	1.653E+00	41	3.727E-05
18	1.353E+00	42	1.068E-05
19	1.003E+00	43	5.044E-06
20	8.208E-01	44	1.855E-06
21	7.427E-01	45	8.764E-07
22	6.081E-01	46	4.140E-07
23	4.979E-01	47	1.000E-07
24	3.688E-01		1.000E-11

**Table 2-2 Summary of Regulatory Positions on Fluence Calculation Methods [1].**

	<u>Regulatory Position</u>
<u>Fluence Determination.</u> Absolute fluence calculations, rather than extrapolated fluence measurements, must be used for the fluence determination.	1.3
<u>Modeling Data.</u> The calculation modeling (geometry, materials, etc.) should be based on documented and verified plant-specific data.	1.1.1
<u>Nuclear Data.</u> The latest version of the Evaluated Nuclear Data File (ENDF/B) should be used for determining nuclear cross-sections. Cross-section sets based on earlier or equivalent nuclear-data sets that have been thoroughly benchmarked are also acceptable. When the recommended cross-section data change, the effect of these changes on the licensee-specific methodology must be evaluated and the fluence estimates updated when the effects are significant.	1.1.2
<u>Cross-Section Angular Representation.</u> In discrete ordinates transport calculations, a $P_3$ angular decomposition of the scattering cross-sections (at a minimum) must be employed.	1.1.2
<u>Cross-Section Group Collapsing.</u> The adequacy of the collapsed job library must be demonstrated by comparing calculations for a representative configuration performed with both the master library and the job library.	1.1.2
<u>Neutron Source.</u> The core neutron source should account for local fuel isotopics and, where appropriate, moderator density. The neutron source normalization and energy dependence must account for the fuel exposure dependence of the fission spectra, the number of neutrons produced per fission, and the energy released per fission.	1.2
<u>End-of-Life Predictions.</u> Predictions of the vessel end-of-life fluence should be made with a best-estimate or conservative generic power distribution. If a best estimate is used, the power distribution must be updated if changes in core loadings, surveillance measurements, or other information indicate a significant change in projected fluence values.	1.2
<u>Spatial Representation.</u> Discrete ordinates neutron transport calculations should incorporate a detailed radial- and azimuthal-spatial mesh of ~2 intervals per inch radially. The discrete ordinates calculations must employ (at a minimum) an $S_8$ quadrature and (at least) 40-80 intervals per octant.	1.3.1
<u>Multiple Transport Calculations.</u> If the calculation is performed using two or more "bootstrap" calculations, the adequacy of the overlap regions must be demonstrated.	1.3.1

**Table 2-2 Summary of Regulatory Positions on Fluence Calculation Methods [1].  
(Continued)**

	<u>Regulatory Position</u>
<u>Point Estimates.</u> If the dimensions of the tally region or the definition of the average-flux region introduce a bias in the tally edit, the Monte Carlo prediction should be adjusted to eliminate the calculational bias. The average-flux region surrounding the point location should not include material boundaries or be located near reflecting, periodic or white boundaries.	1.3.2
<u>Statistical Tests.</u> The Monte Carlo estimated mean and relative error should be tested and satisfy all statistical criteria.	1.3.2
<u>Variance Reduction.</u> All variance reduction methods should be qualified by comparison with calculations performed without variance reduction.	1.3.2
<u>Capsule Modeling.</u> The capsule fluence is extremely sensitive to the geometrical representation of the capsule geometry and internal water region, and the adequacy of the capsule representation and mesh must be demonstrated	1.3.3
<u>Spectral Effects on <math>RT_{NDT}</math>.</u> In order to account for the neutron spectrum dependence of $RT_{NDT}$ , when it is extrapolated from the inside surface of the pressure vessel to the T/4 and 3T/4 vessel locations using the > 1-MeV fluence, a spectral lead factor must be applied to the fluence for the calculation of $\Delta RT_{NDT}$ .	1.3.3
<u>Cavity Calculations.</u> In discrete ordinates transport-calculations, the adequacy of the $S_8$ angular quadrature used in cavity transport calculations must be demonstrated.	1.3.5
<u>Methods Qualification.</u> The calculational methodology must be qualified by both (1) comparisons to measurement and calculational benchmarks and (2) an analytic uncertainty analysis. The methods used to calculate the benchmarks must be consistent (to the extent possible) with the methods used to calculate the vessel fluence. The overall calculational bias and uncertainty must be determined by an appropriate combination of the analytic uncertainty analysis and the uncertainty analysis based on the comparisons to the benchmarks.	1.4.1, 1.4.2, 1.4.3
<u>Fluence Calculational Uncertainty.</u> The vessel fluence (1 sigma) calculational uncertainty must be demonstrated to be 20% for $RT_{PTS}$ and $RT_{NDT}$ determination. In these applications, if the benchmark comparisons indicate differences greater than ~20%, the calculational model must be adjusted or a correction must be applied to reduce the difference between the fluence prediction and the upper 1-sigma limit to within 20%. For other applications, the accuracy should be determined using the approach described in Regulatory Position 1.4, and an uncertainty allowance should be included in the fluence estimate as appropriate in the specific application.	1, 1.4.3

### 3.0 PCA Benchmark Calculation

---

The PCA pressure vessel simulator was constructed to provide a well-characterized geometry that is a mockup of typical reactor geometries. A view of this benchmark facility is shown in Figure 3-1 (from Reference [7]). Measurements were made with this simulator arranged in a variety of geometries, including in some cases simulated surveillance capsules, but the recommended benchmark described in Reference [7] consists of a single geometry. The reference provides a complete description of the benchmark including the geometry and source distribution. The geometry has a 12 cm gap between the reactor core and thermal shield plate, and a 13 cm gap between the thermal shield and the vessel simulator. A schematic of this geometry is shown in Figure 3-2 (from Reference [7]). While this geometry is more typical of PWR geometries than that of BWRs, these are the largest water gaps studied in the PCA. It is felt that this PCA geometry comes the closest to BWR geometry of any recommended benchmark (including recommendations both from RG 1.190 and from ASTM Standard E2006 [19]) and thus is the most applicable for benchmark testing of BWR calculations as applied to the reactor vessel and in-vessel structures. The PCA tests neutron transport calculations both through significant water regions and through steel regions somewhat thicker than BWR vessels. Moreover, the water regions in the PCA are effectively thicker than 12-13 cm since water in the PCA has a density of about 1 compared to about 0.75 in the BWR bypass and downcomer region. Use of the PCA benchmark is also desirable to supplement measurements in actual reactor geometries because it allows validation of neutron transport calculations in regions where dosimetry measurements cannot normally be made. Thus it is concluded that use of the PCA benchmark to test BWR calculational methodology is valuable and satisfies in part the benchmarking requirements of RG 1.190.

Results in the PCA were calculated using X,Y,Z geometry. The results were synthesized from an X,Y calculation (X is the horizontal direction and Y is the direction out from the core through the mockup), a Y,Z calculation (Z is the vertical direction), and a one-dimensional calculation in Y. The synthesis equation is:

$$\phi(X,Y,Z) = \phi(X,Y) * \phi(Y,Z) / \phi(Y).$$

The X,Y model was set up using 79 meshes in the X direction and 130 meshes in the Y direction. The 79 X meshes consist of 17 meshes in the water on each side of the core and 45 meshes within the core. The line of symmetry at X=0 was ignored and the whole width of the core was included in the model. The Y direction starts at the line of symmetry in the middle of the core and extends through to the water at the rear of the void box. The mesh spacing is defined to ensure good convergence of the calculated flux. Similarly, the Y,Z model was set up using the same Y dimensions and meshes and 61 meshes in the vertical direction. The model extends from the water region below the fuel to the water region above the fuel. Both the X,Y and Y,Z models include water regions outside the thermal shield and pressure vessel simulator and thus partially take into account streaming that can occur around these structures due to their finite size.

The fuel region was modeled as a homogeneous material, calculated from the dimensions of the fuel plates and other structures. The fuel elements are made up of slightly curved fuel plates. This curvature was ignored in the model and the fuel elements were taken to have a rectangular cross section (8.100 cm in the Y direction by 7.709 cm in the X direction). The fuel height of the core region was taken to be the fuel element length (62.548 cm), but the source was confined to the length of the fueled region in the fuel plates (60.008 cm).

The power distribution in the horizontal plane was defined by a 3x3 array for each fuel element. This distribution was used directly for the X,Y calculation. In the vertical direction, the power distribution was specified by a cosine function:

$$p(z) = C \cos[B_z(z-z_0)]$$

where C is a normalization constant,  $B_z$  is equal to  $0.0442 \text{ cm}^{-1}$  and  $z_0$  is equal to  $-4.20 \text{ cm}$  [7]. The overall normalization of the calculations is a source of 1 neutron/cm-s produced in the core. The fuel enrichment is 93% U235 and it was assumed that 100% of the fissions were from U235.

Measurements in the mockup can be made by inserting dosimetry into tubes extending down through the water and through the mockup region. Both active and passive dosimetry measurements were made (using several different techniques). Results are available for seven measurement positions ranging from the front of the thermal shield to the back of the vessel. These positions are listed and described in Table 3-1.

All measurements were normalized to a reactor power of one fission neutron per second produced in the core. The measurements were related to similar measurements made in a U235 fission spectrum and are presented in the units of "equivalent fission flux", which is the detector response in the PCA divided by the detector response in a U235 fission flux. By expressing the measurement in this way, a number of uncertainties are eliminated from the measurement (e.g. fission yield, gamma yield, and detector efficiency). Thus, some measurement uncertainties are reported to be as low as 1% or less [7]. Most of the non-fission radiometric dosimeter measurements have uncertainties between 1% and 3%. The fission measurements have higher uncertainties (5% to 9%), which may be due in part to differences in results obtained with the different techniques. The benchmark specifications do not give any estimate of uncertainties in positioning (or reproducibility of positioning) of the mockup, and this could be an important consideration in an uncertainty evaluation of comparisons of calculations with the measurements.

Results were calculated for the measured dosimetry reactions at each of the locations in Table 3-1. The reaction rates were calculated assuming 1 fission neutron per second produced in the core from U235 fission. The reaction rates were then converted to give an equivalent fission flux by dividing by a calculated reaction rate in a unit U235 fission spectrum. An initial analysis was performed using the 47-group dosimetry cross sections in the BUGLE-96 library. These cross sections are all derived based on ENDF/B-VI. As shown in Table 3-2, the C/M results using the BUGLE-96 dosimetry cross sections (C/M column marked "Old (BUGLE)") were consistent except for the rhodium and U238 reactions. Therefore, additional calculations

were performed to better understand the reason for the deviation of the C/M results for these two reactions.

The rhodium reaction is not one that is commonly used in reactor dosimetry analyses because of the very short half-life. Therefore less attention has been paid to the dosimetry cross section for this reaction in the ENDF/B-VI evaluation, and it may not be accurate (as these results indicate). Difficulty with the U238 cross section is due in part to spectrum differences in the threshold region for this reaction that make the 47-group structure too coarse to give as accurate a result as for the other reactions. Therefore, a new analysis was performed as described next.

In ASTM Standard E1018 [20], a recommended dosimetry cross section set is specified in 640 energy groups (SAND group structure). BUGLE has 15 energy groups of varying width between 1 and 10 MeV, while SAND has 90 evenly spaced groups. Accordingly, it was decided to use the SAND II code [21] to evaluate the PCA dosimetry. While SAND II is a code developed to perform spectrum adjustment, no adjustment is being made here. The code is used merely to calculate dosimeter activities using the recommended dosimetry library. To carry this analysis out, the assumption is made that the actual neutron spectrum in the energy region above about 0.1 MeV is fairly smooth. This assumption is justified because the effect of resonances in this region is small. Using this assumption, the SAND II code expands the 47-group calculated neutron spectrum into the SAND finer group structure using a spline procedure to fit the integral fluence rate. The expanded 640 group spectrum can then be multiplied by the 640 group dosimetry cross sections and summed to give the reaction rate. This process minimizes the group structure effects for threshold reactions in energy regions where the dosimetry cross section is rapidly varying. This is particularly important when the threshold region accounts for a large part of the dosimeter response.

Results using the SAND procedure are presented in Table 3-2. This table contains the updated calculated values for the equivalent fission fluxes using the SAND procedure. The calculation to measurement (C/M) ratios for both the old (BUGLE) results and the new (SAND) results are shown. For most of the reactions, the difference is less than 2%. Notable changes did occur for the U238 fission reaction and the Rh(n,n') reaction. In the case of the rhodium, the cause for the change is clear. The BUGLE cross section for the rhodium reaction is derived from ENDF/B-VI and the ASTM recommended dosimetry cross section is taken from IRDF-90 [22]. The IRDF-90 cross section is based on an evaluation that uses dosimetry results to establish its validity. Therefore, it is not surprising that use of this cross section produces agreement with the measurements that are consistent with the results for other dosimeters.

Results for the U238 fission reaction show significant improvement using the new procedure, but the deviation of the U238 C/M ratios from unity still exceeds that for all the other results. They are, however, very close to the C/M ratios for U238 calculated by Remec [7]. This indicates that bias remains in the U238 measurements or cross section compared to the other dosimetry reactions, but the error is within acceptable limits. The change from BUGLE to SAND results is about an 8% C/M improvement, which is about 4 times the change for the other reactions when similarly derived cross sections are used. This may indicate a problem with the

collapsing of the BUGLE cross section for this reaction, but it is sufficient here to conclude that the SAND II procedure using the recommended U238(n,f) cross section produces results within acceptable bounds and consistent with the benchmark document [7].

Use of the SAND II procedure for BWR dosimetry applications has also been tested for the dosimetry reactions of Ni(n,p), Fe(n,p), and Cu(n, $\alpha$ ). Results for these reactions all indicate that changes between the BUGLE and SAND results are very small similar to those observed in the PCA for dosimeters other than Rh and U238.

Average C/M ratios were calculated at each location using all the measurements available for the PCA. These results are shown in Table 3-3. The calculation is consistently low by about 2% to 7%. There is no obvious trend to the bias in going from the location nearest the core to the one at the back of the vessel. Table 3-3 also contains C/M ratios calculated by Remec [7] using BUGLE-93. The MPM C/M ratios are seen to be very consistent with Remec's ratios except at the A7 position which only has the Np237 reaction. At this position, the MPM results here are in better agreement with the measurements. Results calculated using BUGLE-96 are also reported in Reference [13]. Results in this reference using the synthesis approach show a slight increase in bias going through the pressure vessel, and a three-dimensional calculation was made which eliminated this bias. The latter reference did not use the BUGLE-96 dosimetry cross sections and also made comparisons with a slightly different set of measured data. The fact that the three-dimensional calculation eliminated some of the bias illustrates that the synthesis method may contribute some bias due to the finite size of the PCA. However, this would be a small effect in evaluating the fluence within the beltline region of a power reactor where streaming is very small except possibly in the reactor cavity.

The overall conclusion is that the methodology employed here obtains results consistent with calculations performed by qualified NRC contractors and with measurements reported for the PCA. The results show some consistent bias (possibly due to errors in dimensions or source distributions) but this bias is within acceptable tolerance. The results indicate that the calculation produces consistent results in flux variation from the PCA thermal shield through the outside of the vessel.

**Table 3-1 PCA Dosimetry Locations.**

<b>Location</b>	<b>Distance from Core Face of Aluminum Window (cm)</b>	<b>Location Description</b>
A1	12.0	water at front surface of simulated thermal shield
A2	23.8	water at rear surface of simulated thermal shield
A3	29.7	water at front surface of pressure vessel simulator
A4	39.5	1/4 T position in pressure vessel simulator
A5	44.7	1/2 T position in pressure vessel simulator
A6	50.1	3/4 T position in pressure vessel simulator
A7	59.1	void box at rear of pressure vessel simulator

**Table 3-2 Updated Comparison of Calculated and Measured Results for PCA.**

Reaction	Equivalent Fission Flux (n/cm <sup>2</sup> -s)		C/M	
	Measured Results	New Calculated Results	Old (BUGLE)	New (SAND II)
<b>Location A1</b>				
Np237(n,f)	6.64E-06	6.05E-06	0.891	0.911
U238(n,f)	note 1	5.21E-06	note 1	note 1
Rh103(n,n')	5.54E-06	5.37E-06	1.109	0.969
In115(n,n')	5.61E-06	5.17E-06	0.921	0.921
Ni58(n,p)	5.83E-06	5.47E-06	0.937	0.939
Al27(n, $\alpha$ )	7.87E-06	7.28E-06	0.920	0.925
<b>Location A2</b>				
Np237(n,f)	note 1	6.86E-07	note 1	note 1
U238(n,f)	note 1	5.65E-07	note 1	note 1
Rh103(n,n')	note 1	6.17E-07	note 1	note 1
In115(n,n')	6.06E-07	5.64E-07	0.929	0.931
Ni58(n,p)	6.18E-07	5.88E-07	0.949	0.952
Al27(n, $\alpha$ )	1.02E-06	9.47E-07	0.919	0.928
<b>Location A3</b>				
Np237(n,f)	2.27E-07	2.25E-07	0.970	0.992
U238(n,f)	note 1	2.00E-07	note 1	note 1
Rh103(n,n')	note 1	2.01E-07	note 1	note 1
In115(n,n')	1.99E-07	1.94E-07	0.973	0.973
Ni58(n,p)	2.31E-07	2.27E-07	0.977	0.982
Al27(n, $\alpha$ )	4.48E-07	4.35E-07	0.959	0.971
<b>Location A4</b>				
Np237(n,f)	9.27E-08	8.50E-08	0.916	0.916
U238(n,f)	6.11E-08	5.48E-08	0.814	0.897
Rh103(n,n')	7.74E-08	7.75E-08	1.844	1.002
In115(n,n')	5.87E-08	5.80E-08	0.984	0.989
Ni58(n,p)	5.30E-08	5.06E-08	0.951	0.954
Al27(n, $\alpha$ )	1.02E-07	9.71E-08	0.938	0.952
<b>Location A5</b>				
Np237(n,f)	5.18E-08	4.69E-08	0.906	0.906
U238(n,f)	2.74E-08	2.36E-08	0.778	0.863
Rh103(n,n')	4.35E-08	4.18E-08	2.158	0.960
In115(n,n')	2.76E-08	2.65E-08	0.955	0.961
Ni58(n,p)	2.09E-08	1.99E-08	0.948	0.950
Al27(n, $\alpha$ )	4.10E-08	3.91E-08	0.937	0.953

Note 1: Reference 7 does not report measurements at these locations.

**Table 3-2 Updated Comparison of Calculated and Measured Results for PCA.  
(Continued).**

Reaction	Equivalent Fission Flux (n/cm <sup>2</sup> -s)		C/M	
	Measured Results	New Calculated Results	Old (BUGLE)	New (SAND II)
<b>Location A6</b>				
Np237(n,f)	2.70E-08	2.38E-08	0.879	0.881
U238(n,f)	1.12E-08	9.49E-09	0.764	0.847
Rh103(n,n')	2.19E-08	2.08E-08	2.454	0.950
In115(n,n')	1.17E-08	1.13E-08	0.962	0.969
Ni58(n,p)	7.43E-09	7.35E-09	0.987	0.989
Al27(n, $\alpha$ )	1.54E-08	1.48E-08	0.946	0.964
<b>Location A7</b>				
Np237(n,f)	7.25E-09	6.82E-09	0.926	0.941
U238(n,f)	note 1	2.56E-09	note 1	note 1
Rh103(n,n')	note 1	5.85E-09	note 1	note 1
In115(n,n')	note 1	3.09E-09	note 1	note 1
Ni58(n,p)	note 1	2.05E-09	note 1	note 1
Al27(n, $\alpha$ )	note 1	5.05E-09	note 1	note 1

Note 1: Reference 7 does not report measurements at these locations.

**Table 3-3 Comparison of Calculated and Measured Results for PCA.**

<b>PCA Location</b>	<b>MPM Average C/M Ratio<sup>a</sup></b>	<b>ORNL Average C/M Ratio<sup>b</sup></b>
A1	0.933	0.93
A2	0.937	0.92
A3	0.980	0.96
A4	0.952	0.95
A5	0.932	0.92
A6	0.933	0.91
A7	0.941	0.84
<b>Overall Average</b>	<b>0.943</b>	<b>0.93</b>

- a. Results from this work including all measurements from Table 3-2.
- b. Results from Reference [7]. Np results are excluded at the A1 and A3 positions in the ORNL averages due to large deviations attributed to the BUGLE-93 cross section in the thermal range.

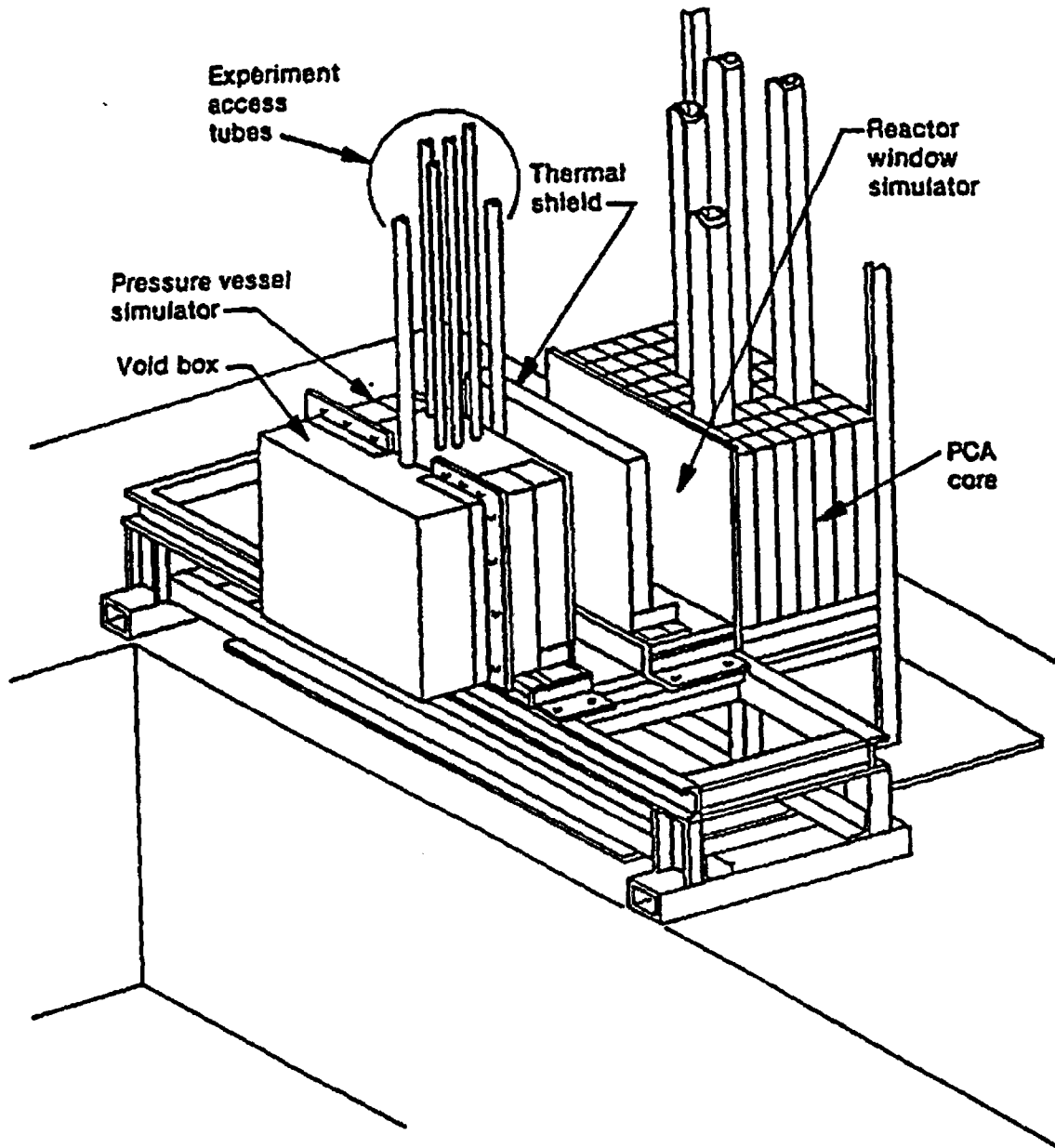


**Figure 3-1 PCA Pressure Vessel Wall Benchmark Facility (Reference [7]).**

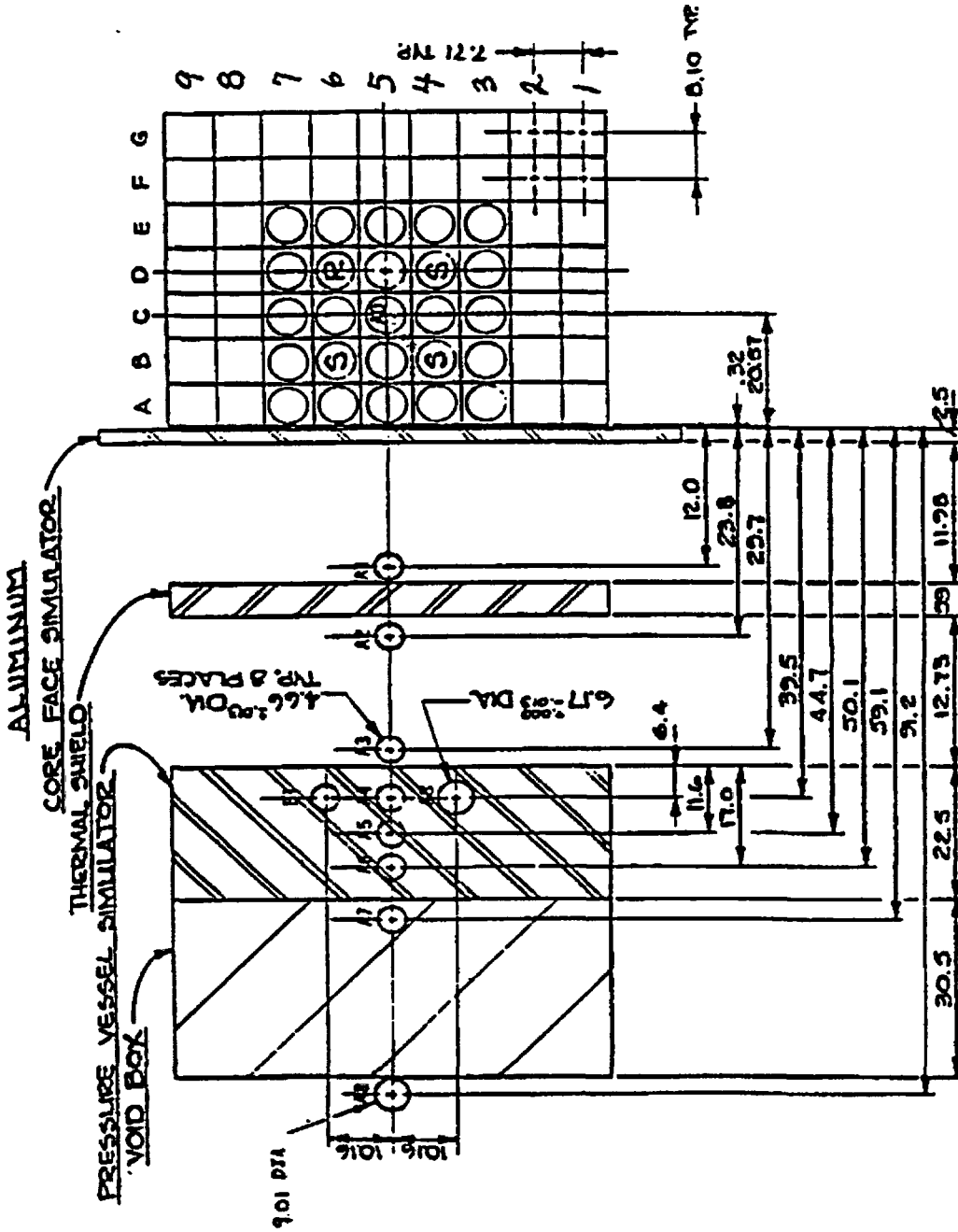


Figure 3-2 Horizontal Cross Section of PCA 12/13 Configuration (Reference [7]).

## **4.0 BWR Computational Benchmark**

---

In addition to benchmarking against measurements, RG 1.190 has a requirement to benchmark the methodology against a calculational benchmark. The calculational benchmarks needed to satisfy this requirement are documented in Reference [8]. Although this reference is a draft report, the final version of this report is not expected to contain any significant differences from the draft version [23]. Therefore, the calculation and comparisons reported here are considered to be final results. It will, of course, be necessary to verify that the final issuance of Reference [8] does not contain significant differences as compared to the draft version which was analyzed in the present work.

The calculational benchmark problems include 3 different PWR geometries and a single BWR problem. It is intended that the analyst select the benchmark problem or problems appropriate to the plant being analyzed. Accordingly, the BWR problem has been calculated since this problem is the one particularly appropriate for NMP-1 and NMP-2 as well as other BWRs. The benchmark problems are designed to ensure that two major difficulties encountered in neutron transport analysis are addressed. First is the strong attenuation of the neutron flux between the edge of the core and the vessel, and through the vessel. This large attenuation makes the vessel fluence dependent on the cross section sets used as well as the numerical procedures to approximate the Boltzmann transport equation. The second calculational difficulty is the evaluation of the neutron source which includes taking into account the irregular (in cylindrical coordinates) core boundary, conversion of the source geometry from X,Y to R, $\theta$  coordinates, and the burnup dependence of the source data. In addition, in the case of the BWR problem, the changing amount of water in the axial direction due to steam formation must be taken into account.

The BWR vessel fluence benchmark problem is for a typical BWR geometry. The core has 800 fuel bundles that have an axial height of 381 cm. Structures between the core and vessel that are included are the shroud, jet pumps and risers, and a surveillance capsule. The model extends outside the vessel into an outer concrete biological shield. The core power distribution and burnup are for a typical equilibrium cycle. The problem specification includes the dimensions of all components, material compositions by region, and the core neutron source.

The layout for the BWR benchmark problem is shown in Figures 4-1 and 4-2 (taken from Reference [8]). The present calculation used 198 radial meshes to represent the region from the center of the core to about 40 cm inside the concrete shield. In the azimuthal direction, 76 meshes were used, and in the axial direction 154 meshes were used to cover the region as shown in Figure 4-2. This mesh meets the requirements specified in RG 1.190 and is sufficiently fine to give an accurate transport result.

The neutron source was calculated from the information provided in the benchmark documentation [8]. This information included the location and fuel burnup for each assembly in the octant representation. Pin powers for the peripheral assemblies were supplied in an 8x8

array. Assemblies one row in from the periphery have the power variation defined in a 4x4 array, and two rows in use a coarser 2x2 array. The assemblies inside the outer three rows are given a flat weighting. Axial power distributions are given in three radial zones for 25 axial segments of the core, each 6 inches in extent. The R,Z model includes the three radial zones and expands the 25 power points into 94 meshes. The meshes are spaced at 2-inch intervals near the middle of the core where the power changes with height are small. Extra mesh points are included near the top and bottom of the core to define the more rapid changes in flux.

The benchmark problem gave fission fractions as a function of fuel burnup. Using these data, the fission fractions were determined using the average burnup for the outer core assemblies. The resultant average fission fractions were used to define the neutron spectrum, the number of neutrons per fission, and the energy per fission. The single neutron spectrum was used for the entire core, but the use of the outer assemblies only to define this spectrum is justified since almost all the neutrons leaking radially out of the core originate in these outer assemblies.

The calculated results were synthesized to produce the flux values and activities in the surveillance capsule and in the reactor vessel. The results were then compared with those tabulated in Reference [8] for the benchmark calculation. These comparisons are summarized in Tables 4-1 through 4-3.

The calculations reported in Reference [8] were carried out using a similar methodology to that used here. In addition, Monte Carlo transport results are reported to confirm the DORT code results. The mesh structure used in the Reference [8] DORT model is detailed, but this mesh was not used in the present calculation. This is because it was desired to check the methodology using the standard methods used by MPM in BWR neutron transport analyses. Another difference from the benchmark calculation in [8] is the use of a different code (DOTSOR rather than MESH) to convert the source from X,Y to R, $\theta$  coordinates. Also, MPM used the BUGLE-96 cross sections rather than the BUGLE-93 cross sections used in the Reference [8] analyses. These differences would be expected to produce variations in calculated flux from the benchmark case, but the results should be within tolerances of 5-10%.

Table 4-1 presents the results for activities calculated in the surveillance capsule which is centered at 3°. These results are interpolated to the radial and azimuthal center of the capsule and are for the maximum axial position in each case. In the present calculation, the axial peak is in the mesh centered at 61 cm above core midplane. However, the difference in activity between this location and the neighboring axial mesh is small. In the benchmark case, the peak is about 66 cm above midplane. The comparisons indicate very good agreement for all the reactions. The non-fission reaction rates agree to within 3%. The fission reactions show a slightly larger difference which is likely due to differences between the BUGLE-96 and BUGLE-93 dosimetry cross sections for these reactions as observed in Reference [7]. The BUGLE-96 dosimetry cross-sections are an improvement over BUGLE-93. Unfortunately, the NUREG analysis used BUGLE-93 cross-sections which leads to differences with the MPM results which are based on BUGLE-96. The existence of these differences is indicated by comparisons in the PCA report [7]. The average ratio for all six reactions is 0.968 with a standard deviation of 0.016.

Tables 4-2 and 4-3 give results for the flux ( $E > 1.0$  MeV) in the vessel. Results are given for the vessel inner radius (IR), at 1/4 thickness (T) intervals through the vessel, and at the vessel outer radius (OR). In Table 4-2, flux results are tabulated for the peak axial position and ratios to the benchmark results are given. The calculated results are very consistent with the benchmark, but do show some scatter. This is presumably due to differences in the source calculation which can affect the relative flux at different angles. The average deviation is about +2%. Variation through the vessel also shows some scatter, but no trends are evident. The scatter in this case is probably due to differences in the model.

Results in the vessel have also been calculated for core midplane. These results are given in Table 4-3. The comparisons with the benchmark calculation are similar to those at the axial maximum. The average deviation is about +3% in this case.

The results of the capsule and vessel comparisons with the benchmark indicate agreement at most points to within  $\pm 5\%$ , with differences slightly larger at some angles. All results agree with the benchmark to within  $\pm 10\%$ . It is concluded that the comparisons between the present calculations and the benchmark calculation are within acceptable tolerances and that the present calculational method applied to BWR geometries is therefore validated.

**Table 4-1 Comparison of Calculated and Benchmark Dosimeter Activities at the Middle of the Surveillance Capsule at the Peak Axial Location.**

<b>Reaction</b>	<b>MPM Calculated Activity</b>	<b>Reference [8] Benchmark Value</b>	<b>Ratio Calculated/Benchmark</b>
U238(n,f)	4.234E-16	4.414E-16	0.959
Np237(n,f)	1.847E-15	1.972E-15	0.936
Ti46(n,p)	3.399E-17	3.464E-17	0.981
Fe54(n,p)	1.481E-16	1.518E-16	0.976
Ni58(n,p)	1.899E-16	1.950E-16	0.974
Cu63(n, $\alpha$ )	2.345E-18	2.387E-18	0.983

**Table 4-2 Comparison of Calculated and Benchmark Results for the Reactor Vessel Calculated at Reactor Axial Peak.**

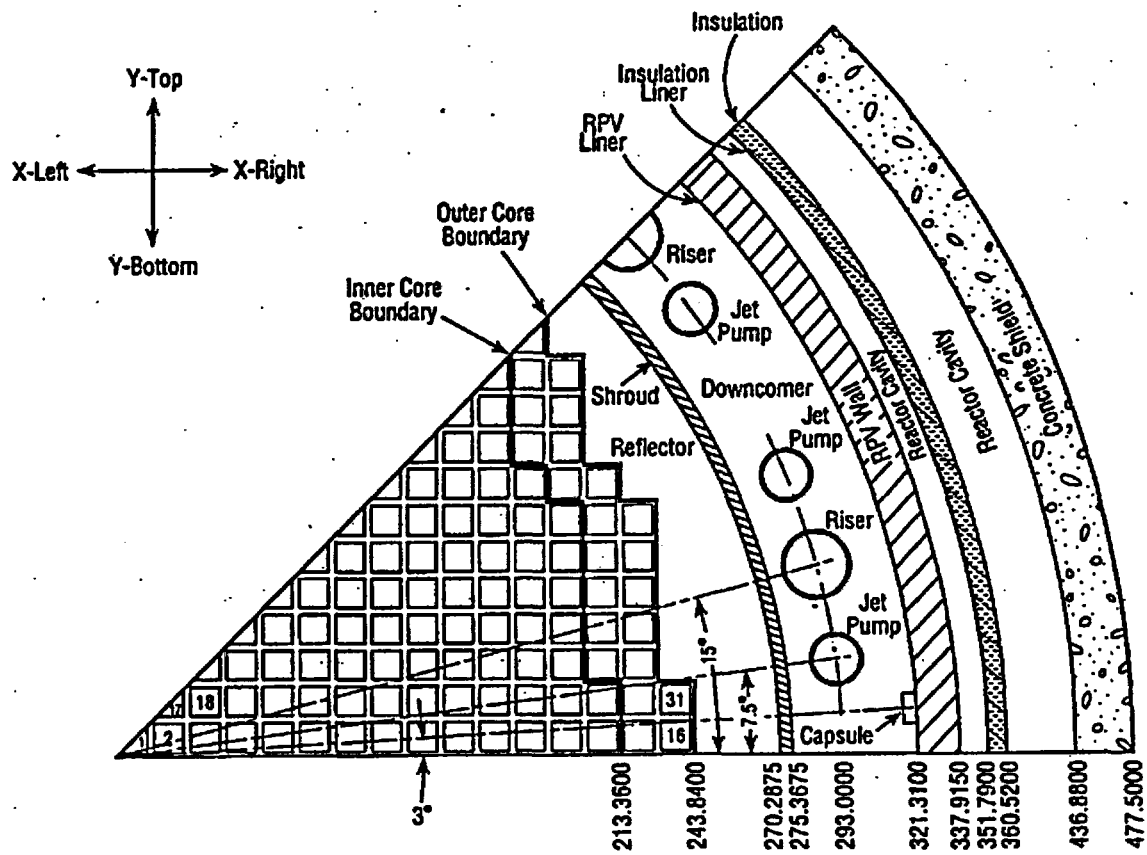
Angle <sup>a</sup>	IR	1/4T	1/2T	3/4T	OR
<b>MPM Calculated Flux (E &gt; 1.0 MeV) n/cm<sup>2</sup>-s</b>					
0	7.738E+08	5.241E+08	3.140E+08	1.782E+08	8.728E+07
15	5.780E+08	3.953E+08	2.417E+08	1.417E+08	7.607E+07
30	1.012E+09	6.892E+08	4.170E+08	2.390E+08	1.168E+08
peak (43)	1.456E+09	9.872E+08	5.916E+08	3.337E+08	1.546E+08
45	1.420E+09	9.629E+08	5.796E+08	3.289E+08	1.535E+08
<b>Reference [8] Benchmark Flux (E &gt; 1.0 MeV) n/cm<sup>2</sup>-s</b>					
0	8.047E+08	5.382E+08	3.207E+08	1.809E+08	8.539E+07
15	5.515E+08	3.810E+08	2.347E+08	1.378E+08	7.253E+07
30	1.015E+09	6.671E+08	4.207E+08	2.405E+08	1.140E+08
peak (43)	1.441E+09	9.679E+08	5.772E+08	3.235E+08	1.459E+08
45	1.323E+09	9.081E+08	5.495E+08	3.185E+08	1.432E+08
<b>Ratio: MPM Calculation/Benchmark Calculation</b>					
0	0.962	0.974	0.979	0.985	1.022
15	1.048	1.038	1.030	1.029	1.049
30	0.997	1.033	0.991	0.994	1.024
peak (43)	1.010	1.020	1.025	1.032	1.060
45	1.073	1.060	1.055	1.033	1.072

a. Results at 0 and 45 degrees are at the center of the initial and final azimuthal mesh. These angles are slightly different for the two calculations. The peak angle refers to the angle with the peak azimuthal flux (about 43 degrees for the present calculation and 42.5 for the benchmark calculation reported in Reference [8]).

**Table 4-3 Comparison of Calculated and Benchmark Results for the Reactor Vessel Calculated at Reactor Axial Midplane.**

Angle <sup>a</sup>	IR	1/4T	1/2T	3/4T	OR
<b>MPM Calculated Flux (E &gt; 1.0 MeV) n/cm<sup>2</sup>-s</b>					
0	7.077E+08	4.798E+08	2.880E+08	1.642E+08	8.185E+07
15	5.286E+08	3.619E+08	2.217E+08	1.305E+08	7.133E+07
30	9.256E+08	6.310E+08	3.825E+08	2.202E+08	1.095E+08
peak (43)	1.331E+09	9.039E+08	5.426E+08	3.074E+08	1.450E+08
45	1.299E+09	8.816E+08	5.316E+08	3.030E+08	1.439E+08
<b>Reference [8] Benchmark Flux (E &gt; 1.0 MeV) n/cm<sup>2</sup>-s</b>					
0	7.267E+08	4.860E+08	2.901E+08	1.641E+08	7.916E+07
15	4.980E+08	3.441E+08	2.122E+08	1.250E+08	6.725E+07
30	9.169E+08	6.268E+08	3.806E+08	2.182E+08	1.057E+08
peak (43)	1.301E+09	8.739E+08	5.222E+08	2.935E+08	1.353E+08
45	1.194E+09	8.198E+08	4.971E+08	2.889E+08	1.328E+08
<b>Ratio: MPM Calculation/Benchmark Calculation</b>					
0	0.974	0.987	0.993	1.001	1.034
15	1.062	1.052	1.045	1.045	1.061
30	1.010	1.007	1.005	1.009	1.036
peak (43)	1.023	1.034	1.039	1.047	1.071
45	1.088	1.075	1.069	1.049	1.084

a. Results at 0 and 45 degrees are at the center of the initial and final azimuthal mesh. These angles are slightly different for the two calculations. The peak angle refers to the angle with the peak azimuthal flux (about 43 degrees for the present calculation and 42.5 for the benchmark calculation reported in Reference [8]).



NOTE: All Dimensions in cm

Figure 4-1 BWR Benchmark Problem Horizontal View (Reference [8]).

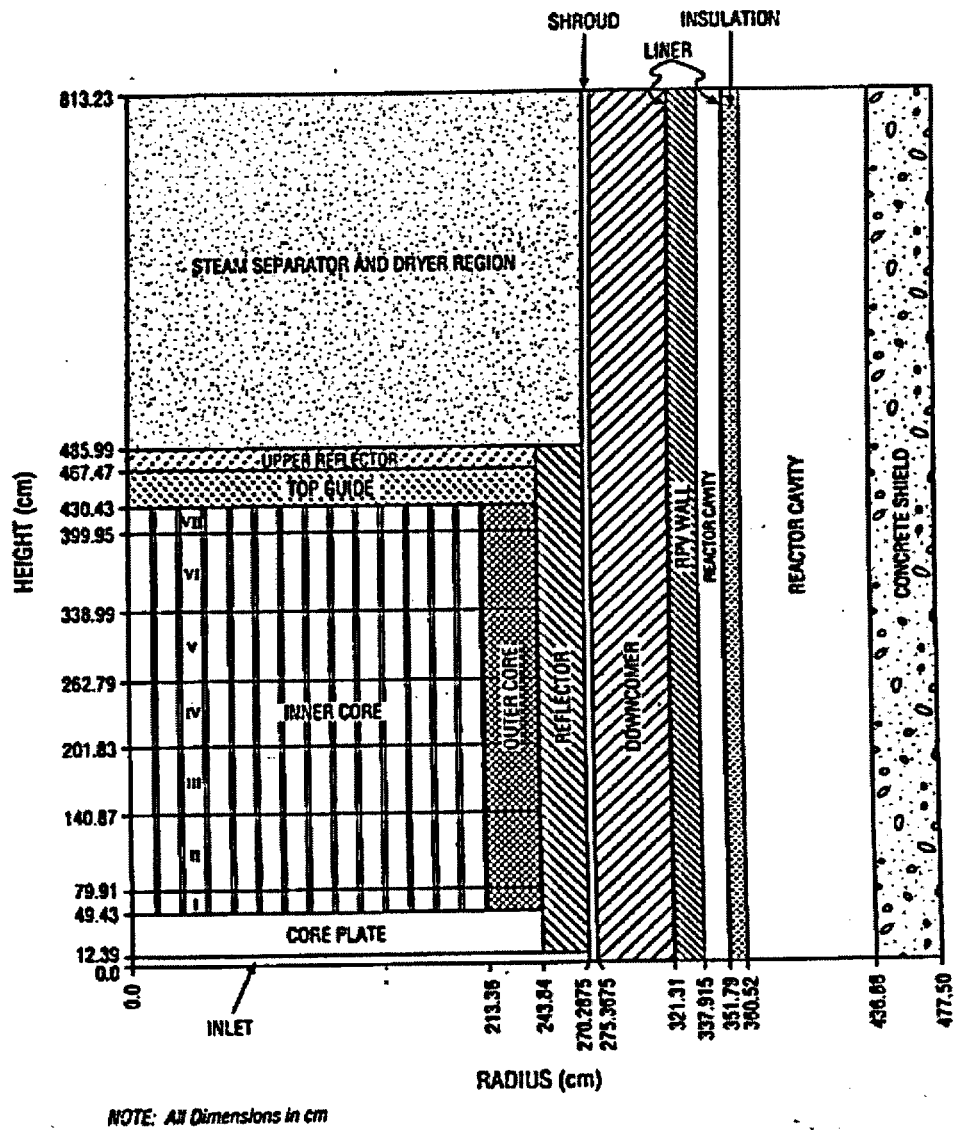


Figure 4-2 BWR Benchmark Problem Axial View (Reference [8]).

## **5.0 Plant-specific Benchmarking**

---

An important part of neutron transport method benchmarking is the comparison of calculation results with dosimetry measurements from the actual plant of interest, or with one that has similar geometry and fuel power distributions. It is, of course, preferred that this element of benchmarking be performed using data from the plant itself. Dosimetry measurement results from both NMP-1 and NMP-2 have been analyzed in order to provide verification of the accuracy of fluence evaluations in these plants. These measurements enable possible errors not detected by the other benchmarking efforts to be identified and properly addressed. Such errors may arise from various sources such as uncertainties in plant dimensions, fuel power distributions, time variations in flux level, and/or void fractions in outer fuel bundles.

### **5.1 NMP-1 Benchmarks**

Surveillance dosimetry removed from NMP-1 consists of the following:

- Dosimetry wires attached to a surveillance capsule removed after the first cycle of operation which ended in April 1973.
- Dosimetry wires contained in the 30° surveillance capsule removed after cycle 5 which ended in March 1979.
- Dosimetry wires contained in the 300° surveillance capsule removed during a cycle 7 shutdown in March 1982.
- Dosimetry wires contained in the 210° surveillance capsule removed after cycle 12 which ended in March 1997.
- Boat samples removed from the inside and outside of the shroud after cycle 12 which ended in March 1997.

Calculations of the latter two sets of measurements were made in 1998 as part of the surveillance capsule report and reports projecting shroud and vessel fluence. Detailed analyses of the first three sets on this list were not made at that time. These sets were not analyzed in detail in the past because the amount of data on the earlier fuel cycles was not nearly as extensive as that on fuel cycle 12. The detailed data needed for this work have recently been provided by Constellation and these dosimetry sets have now all been analyzed and comparisons made to provide additional plant-specific benchmark validation for NMP calculations. Calculations for fuel cycles 7 (an update of the earlier calculation), 9, 10, and 11 were performed. In addition, updated analyses of cycle 12 were carried out to ensure that all the analyses are consistent and use the latest methodology and most recent information. The cycle 12 analysis consisted of 5 cases which spanned the cycle and reflected the time variation of the power distribution and void fraction distribution.

To perform the dosimetry analysis, updated models of the NMP-1 reactor were constructed. Data provided in earlier transmittals [24, 25, 26] were reviewed and the revised models were developed which include the latest information available on the reactor geometry and neutron source ([27] through [34]). Changes from earlier models also include the use of

plant-specific data on regions above and below the core and definition of the regions beyond the vessel into the biological shield. Moreover, a more precise definition of the outer core edge and outer row of fuel bundles was incorporated into the model [30]. The new model also had slightly different radial locations for the capsule and vessel that resulted from further analysis of design and as-built drawings.

The R- $\theta$  model is shown in Figure 5-1. The model included 176 mesh points in the radial direction covering the range from the center of the core to about 12 inches into the concrete biological shield. In the azimuthal direction, 66 mesh points were used to model a single octant of the reactor. Inspection of the fuel loading patterns indicated that only minor deviations from an octant symmetry were present and thus use of a single octant in the model was justified. The core region used a homogenized material distribution which includes the fuel, fuel cladding, and the water. The water region in the fuel was divided into two parts: one with the water in the fuel bundle outside the pins, and one that included the water in the water pins and water in the channels outside the fuel bundle. The latter water was assumed to be all at the base water density with no steam fraction. The other water volume contains both liquid water and steam. The fraction occupied by steam is known as the void fraction and varies by fuel bundle and by axial position within the fuel bundle.

Inspection of the void fraction values indicated that significant variation in the void fraction occurred, but that some groups of neighboring fuel bundles had close to the same void fraction distribution. To model the void fraction variation, the outer row of fuel bundles was divided into six regions of approximately uniform water material density, and the average water density for the assemblies in each of these regions was calculated by multiplying the base water density by 1.0 minus the void fraction. An additional 5 regions contain fuel bundles in the next to outer row. The third to outer row is represented by a single region, and a final region encompasses the remainder of the core.

Since the NMP-1 BWR has large water channels between some of the fuel bundles in order to accommodate the control rods, the core model explicitly accounted for the water channel at the inside and outside of the outer row of fuel bundles. The volume fractions of the outer two rows of fuel bundles were adjusted from the average for the homogenized core to exclude these regions. The water radially outside the outer row of bundles is included in the bypass region, and the water inside this row is included as a water channel.

For the R,Z model, the core was divided into 4 radial regions. Three of these regions consisted of each of the outer three rows of assemblies averaged over the octant. The fourth region consisted of the inner part of the core. The neutron source in each of these regions was calculated using a radial source averaged over the octant together with an average axial power shape for each region. The axial power distribution was supplied for each assembly in 24 or 25 nodes, each representing about 6 inches of core height.

Each of the four radial regions was also divided into axial regions according to variation in void fraction. The void fraction was given for each assembly in 24 or 25 axial nodes. Except for nodes near the bottom of the core which had zero void fraction, each node was modeled as a

separate region for the calculation. This resulted in a total of 88 (or 92 for the 25 node case) varying regions in the core, each with a distinct cross section set. For the R-Z model, the core radius was taken to be that which gave the equivalent core volume. Regions above and below the core were modeled with smeared regions representing water volumes with stainless steel and zirconium regions. The model had 176 mesh points in the radial direction identical to the R- $\theta$  model. In the axial direction, the model had 139 (or 142) mesh points with 91 (94) in the core region.

Analysis of the dosimetry removed from the reactor before the end of cycle 7 was analyzed using the cycle 7 fuel power distribution and axial void fraction distribution in the three dimensions. This cycle was chosen to be most representative of the early operation of NMP-1 and the choice was necessary because information to define the power distribution and void fraction details for the earlier cycles is not available. Use of the approximation that cycles 1 to 6 are identical to cycle 7 produces additional uncertainty in the calculation of dosimetry results. Based on information available for these earlier cycles and on variations in NMP-1 and other BWR plants, this uncertainty is estimated to be 9% ( $1\sigma$ ).

#### *Cycle 1 Dosimetry Analysis*

Results for the cycle 1 dosimetry are presented in Table 5-1 taken from results reported in [35]. This dosimetry set was located in a tube at the right rear of a dosimetry capsule. The set consisted of wires which extended vertically and which were centered at axial midplane. Three samples each of copper and iron wires were counted. Nickel counts are not available because of the long delay which occurred between the end of irradiation and counting. The results shown in Table 5-1 have been decay corrected to the end-of-irradiation date of April 14, 1973.

Since no specific location information is available on the individual wire samples, they were averaged for each dosimeter type. The average results were then compared with calculated dps/mg for each. Comparisons indicate good agreement between measurement and calculation with an overall average C/M of 0.937.

#### *30 Degree Surveillance Capsule Dosimetry Analysis*

The dosimetry results for the 30° capsule are presented in Table 5-2. The capsule was removed from the reactor in 1979, but the dosimetry was not analyzed until 1984 [36]. Thus, due to the short decay half-life, no meaningful data on the nickel wires could be obtained. The capsule had 3 packets of Charpy specimens and each packet had dosimeter wires located at the top of the packet running horizontally across the capsule. It is assumed that the wires are located near to the capsule radial centerline. The axial wire location is determined from the capsule layout, and the resulting locations of the 3 sets span about 5 inches centered slightly above axial midplane. As can be seen from the calculated results in Table 5-2, the differences in flux between the axial positions are relatively small. Table 5-2 contains results for 3 Fe dosimeters and 2 Cu dosimeters. The P1 packet did not contain a copper wire. The measured results in the table are decay corrected to an end-of-irradiation date of March 3, 1979. Results show very good agreement between calculation and measurement with an overall average C/M of 0.996.

### *300 Degree Surveillance Capsule Dosimetry Analysis*

The 300° capsule is similar to the 30° capsule except that only two Charpy packets were irradiated. In this case, the Ni wires could be counted to supplement the Fe and Cu data. Results are shown in Table 5-3 which have been decay corrected to March 19, 1982 [37]. The results again show very good agreement for the Cu monitor, but deviations increase for the Fe and Ni monitors. This may be due, in part, to the fact that the Ni monitors are almost entirely dependent on the flux level throughout fuel cycle 7 (up to the capsule removal), as compared to the Cu which integrates over past cycles. Since the calculation uses conditions at the middle of cycle 7 to represent an average over the cycle, it is not surprising that part of the cycle shows deviations in flux level from the average.

### *210 Degree Surveillance Capsule Dosimetry Analysis*

At the end of NMP-1 fuel cycle 12 (March 3, 1997), the surveillance capsule located at 210° was removed for analysis. This capsule contained Fe, Ni, and Cu dosimeters and the measurement results are reported in Reference [2]. At the same time, in order to determine the material properties of the shroud, and to provide dosimetry data, boat samples were removed from the shroud at two locations. One was cut from the inner diameter (ID) surface of axial weld V9 at an elevation of 26.4 inches above core midplane. This sample was intended to provide near peak flux data for the weld. The other sample was cut from the shroud outer diameter (OD) surface at an elevation of 8.3 inches below core midplane. This sample was intended to provide relatively low flux data. Both samples were taken at azimuthal positions equivalent to 20°. The boat samples were evaluated by Framatome Technologies and the fast fluence was determined based on the Fe54(n,p)Mn54 and Ni58(n,p)Co58 reactions [38]. An inconsistency was found to exist between the Fe and Ni reactions at the boat sample locations. Further, MPM's analysis of the capsule dosimetry indicated, to a lesser extent, an inconsistency in the copper reaction for the capsule. Based on these findings, an in-depth analysis by MPM was performed of both the boat sample and the capsule dosimetry data for cycle 12.

Since the Fe and Ni reactions have a similar neutron response as a function of neutron energy, it was proposed that the most likely cause of the difference between these results is a change in the flux level relative to reactor power at the sample location (i.e. the reaction rate of the dosimeter material with the reactor at full power varies during the fuel cycle). Such a flux level change can occur due to changes in radial or axial power shape, or due to changes in leakage from the core due to water density changes. As fuel burnup occurs, or as reactor control rod patterns change, these types of effects can be expected. Accordingly, a detailed investigation was made of cycle 12 to evaluate the cycle changes that affect the flux level at the dosimetry locations.

Neutron transport calculations were performed for five cases representing different time intervals of cycle 12. The core power distributions and void fractions were calculated by NMP for 68 cases during the fuel cycle. Plots were made of axial power distributions for the corner assembly nearest 20° and for a core average. Inspection of these plots indicated that the

variations were not uniform with time, but significant changes occurred at discrete times, presumably due to changes in operation (such as control rod patterns). To account for these changes, the operating time was divided into 5 intervals which contained cases with similar profiles. A typical case for each interval was then selected from near the middle of that operating period. An R- $\theta$  calculation was then carried out for each case with a midplane neutron source and void fraction distribution calculated for that case. The effect of flux variations in earlier cycles has much less effect on the dosimetry results but, as part of the updated analysis, cycles 9, 10, and 11 were analyzed.

Results from the 210° capsule are shown in Table 5-4. The calculated values use a position dependent flux-time history evaluated by adjusting the reactor power history by the relative calculated flux distribution at each location. The results indicate that, on the average, there is very good agreement with the calculation, although there is a consistent trend of C/M with dosimeter half-life indicating that the detailed cycle 12 analysis may still not completely reflect the changing flux levels that occurred during the cycle. However, all the dosimeters fall well within  $\pm 20\%$  of the measurement.

#### *Shroud Boat Sample Dosimetry Analysis*

The boat samples taken from the NMP-1 shroud contained stainless steel material that extended from the surface of the shroud to about the middle of the shroud wall. Samples for dosimetry analysis were removed from 3 radial locations from each boat sample and analyzed for Mn54 activity from Fe in the steel and Co58 activity from the Ni in the steel, making a total of 12 samples for each weld. Results in units of  $\mu\text{Ci/gm}$  of target isotope (i.e. Fe54 or Ni58) are given in Table 5-5 (taken from reference [39]). This table also provides the radial location of each sample measured from the shroud inner surface. The shroud thickness is 1.5 inches.

The measured disintegration rate ( $\mu\text{Ci/gm}$ ) was converted to dps/mg and these results are compared with calculated values for each measurement in Table 5-5. The calculated values are calculated in a similar manner to those for the surveillance capsule. A summary of the C/M ratio results at each location for Fe and Ni is presented in Table 5-6. The data from Table 5-5 were averaged at each location to produce the data in Table 5-6. Inspection of the results in this table for the upper weld location indicates that the iron results are well predicted (average C/M of 1.05), but the calculated nickel results are biased higher. The average of the Fe and Ni results is 1.079. At the lower weld location, the calculated iron results show an increased bias (C/M = 1.16) and again the Ni calculated results are biased relative to the Fe. The average C/M of the Fe and Ni results at the V10 location is 1.195. For both weld locations, the results at the different radial locations indicate no significant trend in bias going radially out from the core.

Summarizing the cycle 12 results for the capsule and boat sample dosimetry gives the following results:

- Average iron C/M values range from 0.98 in the capsule to 1.16 at the lower boat sample location. All iron measurement values fall within  $\pm 20\%$  of the calculation.
- Copper reaction measurements are only available for the capsule location and show an

average C/M of 0.89.

- Average Ni C/M values are biased with respect to the Fe values by 6-12%. All Ni values fall within  $\pm 20\%$  except at the lower weld location where the C/M values average 1.23.

Fuel cycle 12 was found to be more complicated to analyze than any other NMP fuel cycle encountered, and this is illustrated by the difficulty in obtaining consistent results for the various dosimeters. Breaking up cycle 12 into 5 parts to get a more detailed flux history resulted in substantial improvement in the C/M ratios, but the agreement is still not as good as was obtained for the other dosimetry. This is due in part to several factors. First, even though the cycle was divided into parts with similar power shapes, changes still occur within each model case. It should be noted that the last case encompassed an operating time of 139 calendar days, which is almost two half-lives for the Ni reaction product, Co58. Moreover, this last case produced a relative flux outside the core that was much below the cycle average. At the lower weld location, for example, the relative fast flux was 0.737, a substantial difference from the cycle average. Similar, but somewhat smaller, differences were observed at the other dosimeter locations. If this drop did not occur in a single step, but rather a continuous decline over the last part of the cycle, this would result in overprediction of the Ni reaction rate with only a small effect on the Fe prediction.

A second factor that could cause overprediction of the flux is limitations of the synthesis model. The closest fuel bundle to the shroud at  $20^\circ$  lies at a core corner. The corner fuel bundles have lower power and thus lower void fraction in some axial regions. In the axial model, however, it is not possible to reflect this difference, since the source must be averaged over the azimuthal variation. This effect would result in overprediction of the flux at some angles (e.g.  $20^\circ$ ) at some axial locations, most likely ones below core midplane, and might explain some of the difference between the two shroud weld locations.

Another likely cause of the C/M bias in the boat sample measurements is uncertainty in the azimuthal location of the samples. Since these samples were taken at  $20^\circ$ , and the  $20^\circ$  position is very close to the azimuthal peak (about  $17.5^\circ$ ), the calculated flux can only increase upward by a small amount if the samples were slightly off in the direction of a lower azimuth. However, if the weld sampling occurred at the assumed 5 degree limit of uncertainty, then the calculated flux level could be lower by as much as 30%. Taking into account this uncertainty, together with the estimated uncertainty in the calculation of shroud fluence of 16% [2], it is concluded that observed differences between calculation and measurement do not indicate any significant calculational bias for fluence determination.

In summary, calculated results for the NMP-1 shroud boat samples all fell within  $\pm 20\%$  of the measurement except for the Ni reaction at the lower weld location, which gave a C/M ratio of 1.23. Review of the boat sample data has led to the conclusion that the end-of-cycle power shift toward the top of the core is significant in cycle 12 and causes a decrease in the flux below core mid-plane during the final 6 months of the cycle. This shift is not captured by the 5 case breakdown used to model the average cycle 12 flux calculation. Because of the short half-life, Ni is very sensitive to these end-of-cycle power shift effects. These effects are not significant relative to predicting the cycle average flux as is demonstrated by the good agreement

for the Fe dosimeter for the same location. While it is possible to resolve the Ni dosimeter data with further detailed end-of-cycle 12 analysis, this effort is not considered warranted to qualify the methods or to define the cycle average flux. Therefore, the Ni reaction at shroud weld V10 has been disqualified and the Ni boat sample data have been excluded from the overall C/M ratio calculation for the V10 location. The conclusions reached in previous reports with regard to the boat sample comparisons remain unchanged. Accordingly, the overall C/M ratio for the boat samples has been shown to be less than  $\pm 20\%$  and the Ni reaction at V10 is not needed to determine the cycle average flux nor to qualify the NMP plant-specific fluence calculational methodology. The final C/M ratios for the boat samples are given in Table 5-7.

## 5.2 NMP-2 Benchmark

The NMP-2 3° surveillance capsule was removed at the end of the seventh fuel cycle (March 3, 2000) and the dosimetry was analyzed as part of the surveillance program. This dosimetry consisted of two iron wires and two copper wires. To analyze the dosimetry, a detailed analysis of reactor operation was performed to evaluate changes in neutron flux level at the dosimetry location due to changes in fuel composition, power distributions within the core, and water void fraction. These changes occur between fuel cycles due to changes in fuel loading and fuel design, and within a fuel cycle due to fuel burnup and resultant changes in power shape, control rod position, fission contributions by nuclide, and void fraction vs. axial height in each fuel bundle. For the fuel cycle preceding the capsule removal (cycle 7), five cases were selected to characterize changes during the cycle. These points were distributed throughout the cycle so that each of these was taken to represent an average of the neutron flux level for about 1/5 of the operating time for the cycle. For the other fuel cycles, which have less effect on the dosimetry results, the assumption was made that conditions at the middle of each cycle were an adequate estimation of the average over the cycle and a single calculation was performed for each of these cycles.

The layout for the R- $\theta$  calculation is shown in Figure 5-2. In this figure, all structures outside the core were modeled with a cylindrical symmetry except for the inclusion of a surveillance capsule centered at 3° and jet pump structures located in the downcomer region. The latter are not to scale in the figure. The jet pumps are only approximate models of two pumps with a central pipe (riser) in between.

The R- $\theta$  model included 186 mesh points in the radial direction covering the range from the center of the core to ten inches into the biological shield. This large number of mesh points was used to accurately calculate the neutron flux transport from the core edge to the outside of the vessel. In the azimuthal direction, 48 mesh points were used to model a single octant of the reactor. Inspection of the fuel loading patterns indicated that only minor deviations from an octant symmetry were present and these were ignored. The 48 points provided good definition of the variation of the core edge with angle and defined the azimuthal flux variation.

The core region used a homogenized material distribution which includes the fuel, fuel cladding, and the water. The water region in the fuel contains both liquid water and steam. The fraction occupied by steam is known as the void fraction and varies by assembly and axial

position within the fuel. Inspection of the void fraction values indicated that while some assemblies exhibit significant variation in the void fraction, some groups of neighboring assemblies had close to the same void fraction. To model the void fraction variation in the R- $\theta$  model, the outer rows of assemblies were divided into seven regions of approximately uniform water material density, and the average water density for the assemblies in each of these regions was calculated by multiplying the base water density (0.7365 g/cc) by 1.0 minus the void fraction. The assemblies in each of these regions are indicated by the region numbers defined in Figure 5-2. Each one of these regions had a void fraction assigned as the average midplane void fraction value for the assemblies in the region. These average void fraction values were different for each case analyzed.

Water density in the bypass region was varied between 0.7585 g/cc at the inlet and 0.7394 g/cc at the outlet. The value at midplane was taken to be an average of these values. The downcomer water density was calculated for a temperature of 534 °F and a pressure of 1037 psia.

The source calculations used the appropriate power distribution for all the fuel bundles in the first octant together with pin power distributions for the outer rows of bundles. The pin power distributions were used to model the spatial variation of the source within the bundles and took into account the gaps between bundles and water rods in the center. Equal pin power weighting was used for interior fuel bundles. In the calculations, the variation in relative pin power distributions within similar bundles between cycles was determined to be small [4] and so the cycle 7 9x9 mid-cycle pin power distributions were used in the calculations for all the cases. The neutron source per group was defined by an average fission spectrum calculated for a fission breakdown by isotope determined for the average burnup of the outer assemblies for each case. This is a good approximation to the fission spectrum because the outer assemblies were all assemblies with similar burnup, and the fission spectrum only slowly varies with burnup. Almost all of the neutrons that reach the capsule and vessel originate in the outer rows of fuel bundles.

The ORIGEN 2.1 code [12] was used to calculate the effects of burnup on the neutron source. This was carried out using an ORIGEN BWR cross section library appropriate for high burnup fuel. The results were validated by comparison to NMP-2 calculated fuel compositions as a function of fuel burnup. The initial fuel composition for each cycle was taken to be the average initial composition for the outer assemblies. The effects of the varying axial initial enrichment, burnup, and void fraction were ignored in this calculation and are assumed to have negligible impact because the effects of the change in parameters are minor. The ORIGEN code calculated the fission fraction by isotope and the average energy deposited in the reactor per fission ( $\kappa$ ). The isotopic fission fractions were used to determine the fission spectrum and the average number of neutrons per fission ( $\nu$ ). The normalization of the neutron source in the DORT calculations is directly proportional to  $\nu/\kappa$  which slowly varies with burnup.

For the calculation in R-Z geometry, the core was divided into 3 radial regions. Two of these regions consisted of each of the outer two rows of assemblies averaged over the octant. The third region consisted of the inner part of the core. The neutron source in each of these regions was calculated using a radial source averaged over the octant together with an average

axial power shape for each region. The axial power distribution was supplied for each assembly in 25 nodes, each representing 6 inches of core height. Neutron source outside the equivalent core radius was eliminated.

Each radial region was also divided into axial regions according to variation in void fraction. The void fraction was also given for each assembly in 25 axial nodes. Except for nodes near the bottom of the core which had zero void fraction, each node was modeled as a separate region for the calculation. This resulted in a total of 70 regions in the core, each with a distinct cross section set. In addition, the GE11 fuel bundles contain 8 part length fuel pins that end at 96 inches above the bottom of the active fuel. The volume of these pins was replaced with water at axial meshes above the 96 inch level. The bypass region was also modeled with a varying axial water density. The bypass region was divided into 12 subregions within the core height, each with a different water density.

For the R-Z model, the core radius was taken to be that which gave the equivalent core volume. Since the focus of the calculations was on obtaining accurate results at shroud and vessel locations within the beltline axial region, the regions above and below the core in the R-Z model were not modeled using an exact representation of the structures above and below the beltline region. The model was extended above and below the core for 12 inches (30 cm) to provide a reflector region and to allow leakage out to the shroud and vessel. The region below the core (which corresponds to the core plate region in NUREG/CR-6115) was approximated by water with the same density as the downcomer, in contrast to the NUREG model which had a mixture of stainless steel and water. Omission of the stainless steel is conservative for high energy neutron transport. Similarly, the region above the core was approximated using water with the density determined using the core outlet water density. The model had 186 mesh points in the radial direction as in the R- $\theta$  model except with slightly different boundaries near the core edge. In the axial direction, the model had 68 mesh points with 38 in the core region. Further details of the calculations are given in Reference [3].

### *3 Degree Surveillance Capsule Dosimetry Analysis*

The dosimetry results that relate to fast fluence are given in Table 5-8 [3]. The dosimeter measurements are presented in units of disintegrations per second per milligram (dps/mg), adjusted to the end-of-irradiation (March 3, 2000 at 14:17 EST). Using the power history and the reaction rates for Fe and Cu determined by the DORT calculation for each cycle and the five cycle 7 cases, the activity at the end of the irradiation was calculated for a point at the geometrical center of the capsule. The results were obtained by multiplying the calculated reaction rate for each of the two reactions (obtained from the synthesis procedure for each case) by the effective full power seconds (EFPS) for each monthly time interval and then accounting for radioactive decay during the interval and to the end-of-irradiation time.

The location of the dosimeter wires in the NMP-2 3° capsule is uncertain. Unlike most PWR capsule designs, the BWR dosimeters are not placed in sealed containers inside the capsule. Instead, the bare wires are held by spring load near the top or bottom of the capsule for most BWR capsules. The C/M ratios for each dosimeter measurement and the average are

summarized in Table 5-8. For comparison purposes, the C/M ratios were computed at the capsule center and at the best estimate position. The average C/M ratio of 1.07, based on the assumption that the dosimetry is at the capsule center, indicates good agreement between the calculation and the measurement. However, the Fe and Cu dosimetry results do show a large difference with the Fe showing a C/M over 20 %. It should be noted that 95% of the iron response is from the last two irradiation cycles, while 48% of the copper response is from earlier cycles. In addition, copper has a much higher reaction threshold and so only responds to a small fraction of the fast neutrons while the iron responds to a larger fraction. In addition, the copper cross section is not as well known as the iron cross section. Since these observations are not expected to explain all of the discrepancy, additional measurements and analyses were made to better quantify the C/M ratio.

For NMP-2, the intended location is near the front top of the capsule at the right side as viewed from the core. This would place the dosimeters at about 0.48 cm towards the core from the capsule radial center and about 6 inches above core midplane. The radial correction would increase the calculated activity by 4.6% for copper and 7.4% for iron. The axial correction varies during the fuel cycle and between cycles, but the activities 6 inches above midplane average about 4% higher. The azimuthal difference is small, but the activity to the right (higher angles in the first octant) increases by about 1% from that at the center of the capsule. If all these factors are included, the calculated copper activity at the indicated dosimeter position is higher by about 10% compared to the capsule center and the iron by 13%. This results in average C/M ratios of 1.02 for copper and 1.37 for iron, and an average C/M of 1.19.

However, it may also be postulated that the copper dosimeter is positioned towards the core side of the capsule, while the iron is positioned towards the vessel side. This condition could occur if the dosimeters were installed in these positions, shifted during capsule assembly, or if the dosimeters moved during irradiation in the plant. If this assumption is made, then the iron average C/M ratio is 1.19 and the average of the two dosimeter types is 1.11. It is also possible to assume that the dosimeter wires dropped to the bottom of the capsule. This would lower the calculated activity by 4% compared to the capsule axial midplane (instead of increasing it as noted above for the correction to the top of the capsule). The average C/M ratio would then be about 1.02.

### *Charpy Bar Dosimetry Analysis*

Since the bottom of the NMP-2 capsule was cut during capsule disassembly and the wires were located somewhere in the capsule above the cut location, it is not possible to determine the dosimeter wire locations during irradiation. Therefore, to reduce the dosimeter location uncertainty and to obtain a meaningful C/M ratio, an additional measurement was made using a sample cut from a Charpy bar. The sample was a complete slice across the specimen taken near the fracture surface, and thus is radially centered and located very near the azimuthal center of the capsule. The sample was modeled at the radial center of the capsule because the counting geometry for the slice approximates a point source at the radial center. Unfortunately, the axial location within the capsule could not be determined because the specimens were not recorded for axial position during disassembly. This is not a serious problem because the axial uncertainty is

only a few percent. The measurement result, adjusted to the reference time, is 30.62 dps/mg. The Charpy is not pure iron, but has been determined to have an iron fraction of 0.9694. Using this value, the dps/mg of iron is then 31.59. This result is 12% higher than the result from the iron dosimeters and gives a C/M ratio of 1.08. This indicates that the iron dosimeters are located towards the rear of the capsule, and most likely at the bottom. The results using this location for the iron dosimeter, and assuming the copper location towards the core, are shown in the last column of Table 5-8. The average C/M for copper is 0.95 and for iron is 1.09, for an overall average of 1.02, indicating excellent agreement of the calculation with measurement.

Uncertainty in the calculation and measurement is considered in detail in Reference [3]. The uncertainty in the calculated flux at the center of the surveillance capsule was evaluated to be 15.3%. Uncertainty in the measured result must include the uncertainty in activity measurements, dosimeter position uncertainty, dosimeter cross section uncertainty, and the flux history uncertainty. The activity measurements have a total uncertainty of about 3%. As discussed above, the dosimeter position uncertainty can be as large as 10-13%. However, use of the Charpy measurement, which has a better known position, reduces this uncertainty to about 5%. The dosimeter cross section uncertainty is limited by correlation with benchmark measurements. It can be assumed that typical iron and copper reaction integral cross sections are known to within 3% [40]. The flux history uncertainty will vary with the half-life, but can be conservatively assumed to be less than 8% [3]. The total uncertainty in the measurement relative to the calculation is then about 10%. It is seen that the Charpy bar C/M value of 1.08 is well within both the measurement uncertainty and the calculation uncertainty. It is concluded that the measurement provides an excellent validation of the adequacy of the calculation.

### 5.3 Summary of Plant-Specific Benchmark Results

Comparisons were made with surveillance capsule measurements in NMP-1 and NMP-2 and with shroud measurements in NMP-1. For the four sets of NMP-1 capsule dosimetry, all of the calculated dosimeter activities fall well within  $\pm 20\%$  of the measurement. Moreover, if the four sets are averaged, the average C/M result is very close to 1.0. Similar consistency is obtained for the NMP-2 capsule. In all the capsule cases, agreement with measured results within uncertainty was obtained and uncertainties were shown to be less than  $\pm 20\%$ . This meets the criterion set by RG 1.190 for acceptability of the calculations.

For the NMP-1 shroud boat sample measurements, calculated results all fell within  $\pm 20\%$  of the measurement except for the Ni reaction at the lower weld location. The cause of the V10 boat sample Ni C/M ratio being 1.23 is well understood. Finer subdivision of the last cycle would be necessary to accurately model the power and void variations for resolution of the relatively short half-life Ni reaction. The effort associated with analysis of cycle 12 in greater detail, with finer steps though the cycle, is not warranted for resolution of this one reaction. Accordingly, the Ni reaction at V10 has been disqualified and the overall C/M ratio for the boat samples has been shown to be less than  $\pm 20\%$ .

**Table 5-1 Comparison of Calculated and Measured Results for NMP-1 Dosimetry Removed After Cycle 1.**

Dosimeter	Measured dps/mg	Calculated dps/mg	C/M
Fe	95.37	Note 1	Note 1
Fe	94.54	Note 1	Note 1
Fe	103.87	Note 1	Note 1
Fe Average	97.93	94.92	0.969
Cu	5.93	Note 1	Note 1
Cu	5.89	Note 1	Note 1
Cu	5.98	Note 1	Note 1
Cu Average	5.935	5.368	0.905
Overall Average of Cu and Fe			0.937

End-of-irradiation-April 14, 1973.

Note 1: Since no specific location information is available on the individual wire samples, they were averaged for each dosimeter type.

**Table 5-2 Comparison of Calculated and Measured Results for NMP-1 Dosimetry Removed from 30° Capsule.**

Dosimeter	Set ID	Measured dps/mg	Calculated dps/mg	C/M
Fe	P1	188.30	175.92	0.934
Fe	P2	177.72	175.78	0.989
Fe	P3	173.49	175.69	1.013
Fe Average				0.979
Cu	P2	18.05	17.61	0.975
Cu	P3	16.76	17.59	1.050
Cu Average				1.012
Overall Average of Cu and Fe				0.996

End-of-irradiation-March 3, 1979

**Table 5-3 Comparison of Calculated and Measured Results for NMP-1 Dosimetry Removed from 300° Capsule.**

Dosimeter	Set ID	Measured dps/mg	Calculated dps/mg	C/M
Fe	P7	174.10	178.24	1.024
Fe	P8	157.46	178.14	1.131
Fe Average				1.078
Ni	P7	2737	3069.19	1.121
Ni	P8	2641	3067.33	1.161
Ni Average				1.141
Cu	P7	20.80	20.78	0.999
Cu	P8	20.80	20.76	0.998
Cu Average				0.999
Overall Average of Fe, Ni, and Cu				1.073

End-of-irradiation-March 19, 1982.

**Table 5-4 Comparison of Calculated and Measured Results for NMP-1 Dosimetry Removed from 210° Capsule.**

Dosimeter	Measured dps/mg	Calculated dps/mg	C/M
Cu-1	20.66	18.10	0.876
Cu-2	20.81	18.10	0.870
Cu-3	19.43	18.10	0.932
Cu Avg	20.3	18.10	0.892
Fe-1	149.4	139.0	0.930
Fe-2	138.6	139.0	1.003
Fe-3	135.7	139.0	1.024
Fe Avg	141.2	139.0	0.984
Ni-1	1725	1838	1.066
Ni-2	1636	1838	1.124
Ni-3	1592	1838	1.155
Ni Avg	1651	1838	1.113
Capsule Average			0.997

End-of-irradiation-March 3, 1997.

**Table 5-5 Tabulation of NMP-1 Shroud Boat Sample Dosimetry Results.**

Weld V9	Dosimeter Identification	Location* in Shroud (in)	Measured Activity (uCi/g)	Measured Activity (dps/mg)	Calculated Activity (dps/mg)	C/M
1	Fe	0.000	1.94E+04	7.178E+05	7.396E+05	1.030
2	Fe	0.000	1.93E+04	7.141E+05	7.396E+05	1.036
3	Ni	0.000	2.01E+04	7.437E+05	8.697E+05	1.169
4	Ni	0.000	2.15E+04	7.955E+05	8.697E+05	1.093
5	Fe	0.337	1.60E+04	5.920E+05	6.489E+05	1.096
6	Fe	0.337	1.68E+04	6.216E+05	6.489E+05	1.044
7	Ni	0.337	1.91E+04	7.067E+05	7.661E+05	1.084
8	Ni	0.337	1.83E+04	6.771E+05	7.661E+05	1.131
9	Fe	0.850	1.31E+04	4.847E+05	5.044E+05	1.041
10	Fe	0.850	1.32E+04	4.884E+05	5.044E+05	1.033
11	Ni	0.850	1.44E+04	5.328E+05	5.979E+05	1.122
12	Ni	0.850	1.51E+04	5.587E+05	5.979E+05	1.070
Weld V10	Dosimeter Identification	Location* in Shroud (in)	Measured Activity (uCi/g)	Measured Activity (dps/mg)	Calculated Activity (dps/mg)	C/M
1	Fe	0.882	8.98E+03	3.323E+05	3.954E+05	1.190
2	Fe	0.882	9.14E+03	3.382E+05	3.954E+05	1.169
3	Ni	0.882	9.72E+03	3.596E+05	4.364E+05	1.214
4	Ni	0.882	9.91E+03	3.667E+05	4.364E+05	1.190
5	Fe	1.063	8.34E+03	3.086E+05	3.577E+05	1.159
6	Fe	1.063	8.26E+03	3.056E+05	3.577E+05	1.171
7	Ni	1.063	8.42E+03	3.115E+05	3.950E+05	1.268
8	Ni	1.063	8.52E+03	3.152E+05	3.950E+05	1.253
9	Fe	1.500	6.74E+03	2.494E+05	2.815E+05	1.129
10	Fe	1.500	6.74E+03	2.494E+05	2.815E+05	1.129
11	Ni	1.500	6.75E+03	2.498E+05	3.101E+05	1.241
12	Ni	1.500	6.80E+03	2.516E+05	3.101E+05	1.232

a. measured from shroud ID surface

**Table 5-6 Summary of Measured and Calculated Boat Sample C/M Ratios from Nine Mile Point Unit 1 Showing Average Values for Each Dosimetry Location.**

Radial Location <sup>a</sup> (in)	Axial Location <sup>b</sup> (in)	C/M Ratio	
		Fe	Ni
<b>Vertical Weld V9</b>			
0.000	26.4	1.033	1.131
0.337	26.4	1.070	1.108
0.850	26.4	1.037	1.096
Average C/M		1.047	1.112
<b>Vertical Weld V10</b>			
0.882	-8.3	1.180	1.202
1.062	-8.3	1.165	1.261
1.500	-8.3	1.129	1.237
Average C/M		1.158	1.233

- a. Measured from shroud ID surface.
- b. Measured from fuel axial midplane.

**Table 5-7 Summary of Measured and Calculated Boat Sample C/M Ratios from Nine Mile Point Unit 1 Showing Average Final Values for Each Dosimetry Location and Overall Averages.**

Radial Location <sup>a</sup> (in)	Axial Location <sup>b</sup> (in)	C/M Ratio	
		Fe	Ni
<b>Vertical Weld V9</b>			
0.000	26.4	1.033	1.131
0.337	26.4	1.070	1.108
0.850	26.4	1.037	1.096
<b>Vertical Weld V10</b>			
0.882	-8.3	1.180	- <sup>c</sup>
1.062	-8.3	1.165	- <sup>c</sup>
1.500	-8.3	1.129	- <sup>c</sup>
<b>Average C/M</b>		1.102	1.111

- a. Measured from shroud ID surface.
- b. Measured from fuel axial midplane.
- c. V10 Ni results disqualified.

**Table 5-8 Tabulation of NMP-2 3° Surveillance Capsule Dosimetry Results [3,4].**

<b>Dosimeter</b>	<b>Measured Activity (dps/mg)</b>	<b>Calculated Activity (dps/mg) <sup>a</sup></b>	<b>Ratio (C/M) <sup>a</sup> Capsule Center Assumption</b>	<b>Ratio (C/M) <sup>b</sup> Best Estimate Position</b>
Cu-1	4.97	4.50	0.91	0.92
Cu-2	4.62	4.50	0.97	0.99
Avg Cu	4.80	4.50	0.94	0.95
Fe-1	27.84	34.10	1.22	1.10
Fe-2	28.49	34.10	1.20	1.08
Avg Fe	28.16	34.10	1.21	1.09
Capsule Average			1.07	1.02
Charpy Bar (Slice Near Fracture Surface)	31.59 <sup>c</sup>	34.10	1.08 <sup>c</sup>	N/A

End-of-irradiation-March 3, 2000.

- a. There is uncertainty in the NMP-2 capsule dosimetry location. The results in this column are based on the assumption that the dosimetry is at the capsule center.
- b. The results in this column are based on the assumption that the dosimetry is at the best estimate positions. Dosimetry results from the Charpy bar indicate that the dosimetry wires may have moved from their intended locations within the capsule.
- c. The Charpy bar dosimetry results have been corrected for iron composition. A slice was taken from the Charpy bar parallel to and near fracture surface. This approach resulted in an approximate point source near the radial and azimuthal center of the capsule.

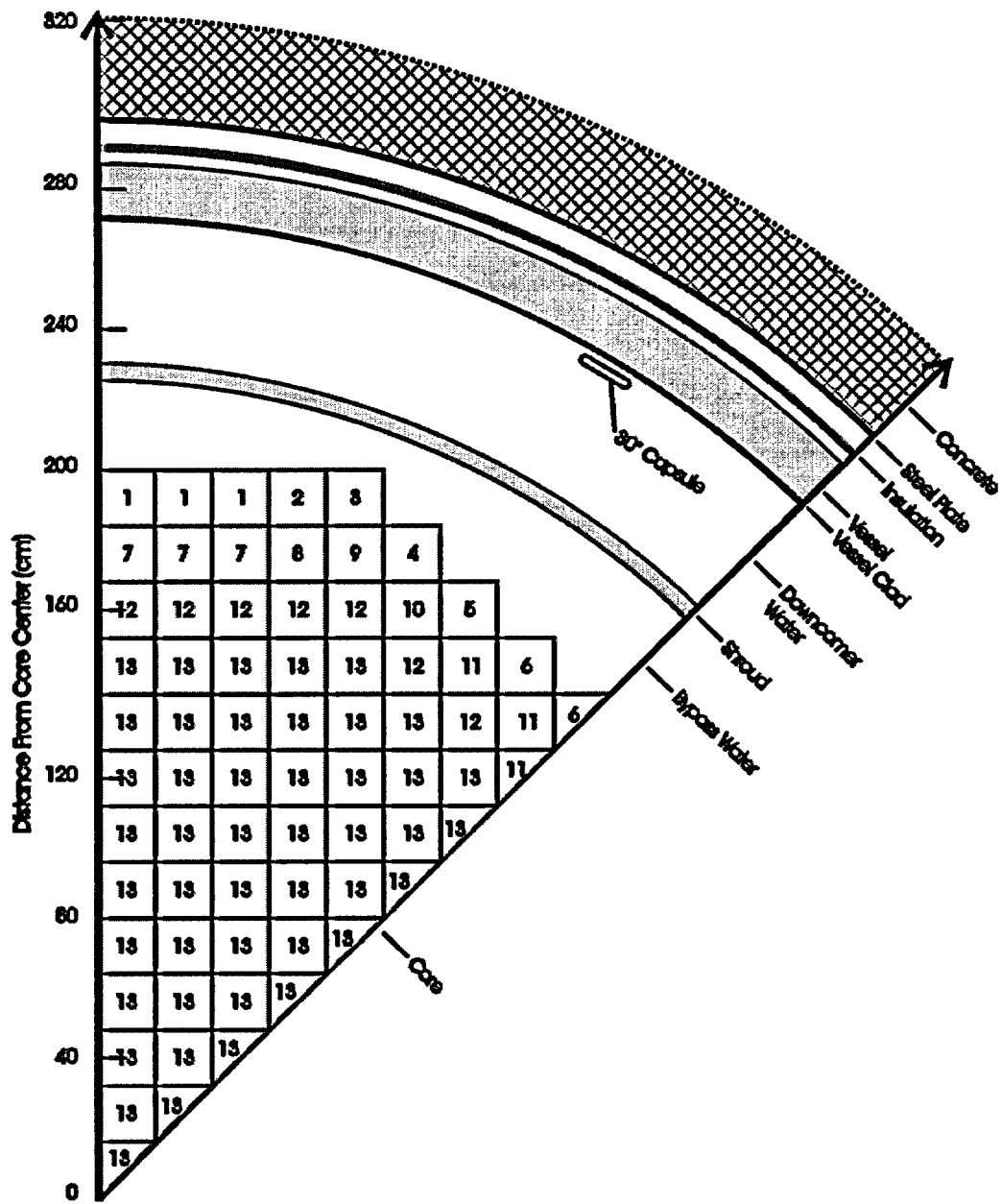


Figure 5-1 Nine Mile Point Unit 1 R-θ Geometry Used in the DORT Calculations. (capsule not drawn to scale)



## 6.0 Summary and Conclusions

---

In order to meet the methods qualification requirements of RG 1.190, the MPM calculational methodology used for Nine Mile Point Unit 1 (Reference 2) and Unit 2 (References 4, 5, and 6) has been validated by comparison with measurement and calculational benchmarks. These include the PCA pressure vessel simulator benchmark, which has high-accuracy measurement results extending from inside a simulated thermal shield through to the outside of a simulated vessel. The calculational results in the PCA show a slight consistent bias (about 6%) with respect to the measurements, but no significant change in bias is observed with change in irradiation position. This indicates that the transport methodology is calculating the flux attenuation outside the core region with high accuracy. The observed bias is consistent with that obtained by other synthesis calculations.

The calculational benchmark was a typical BWR geometry similar to those for NMP-1 and NMP-2. Comparisons were made between the MPM calculations and the benchmark calculational results which indicated very good agreement. In the capsule, the average results were about 3% low, and at the vessel IR and within the vessel the average results were about 2-3% high. All compared results fell within  $\pm 10\%$ .

Additional comparisons were made with surveillance capsule measurements in NMP-1 and NMP-2 and with shroud measurements in NMP-1. For the four sets of NMP-1 capsule dosimetry, all of the calculated dosimeter activities fall well within  $\pm 20\%$  of the measurement. Moreover, if the four sets are averaged, the average C/M result is very close to 1.0. Similar consistency is obtained for the NMP-2 capsule. In all the capsule cases, agreement with measured results within uncertainty was obtained and uncertainties were shown to be less than  $\pm 20\%$ . This meets the criterion set by RG 1.190 for acceptability of the calculations.

For the NMP-1 shroud boat sample measurements, calculated results all fell within  $\pm 20\%$  of the measurement except for the Ni reaction at the lower weld location, but this was within the estimated uncertainty due to calculational accuracy and sample location.

On the basis of the above results it is concluded that for BWR calculations within the beltline region and between the core and the vessel there is no significant bias. Thus no bias factor will be applied to the calculations. In all cases, agreement with measured results within uncertainty was obtained. Uncertainties were shown to be less than  $\pm 20\%$ . This meets the criterion set by RG 1.190 for acceptability of the calculations.

As a result of the work performed and documented in this report, it is concluded that the RG 1.190 requirement for qualification of the MPM methodology used for Nine Mile Point Unit 1 (Reference 2) and Unit 2 (References 4, 5, and 6) by comparisons to measurement and calculational benchmarks has been fully satisfied.

## **7.0 Nomenclature**

---

<b>BWR</b>	<b>boiling water reactor</b>
<b>C/M</b>	<b>calculated-to-measured ratio</b>
<b>dpa</b>	<b>displacements per atom</b>
<b>EFPS</b>	<b>effective full power seconds</b>
<b>ID</b>	<b>inner diameter</b>
<b>IR</b>	<b>inner radius</b>
<b>LWR</b>	<b>light water reactor</b>
<b>MPM</b>	<b>MPM Technologies, Inc.</b>
<b>NMP-1</b>	<b>Nine Mile Point Unit 1</b>
<b>NMP-2</b>	<b>Nine Mile Point Unit 2</b>
<b>NRC</b>	<b>U. S. Nuclear Regulatory Commission</b>
<b>OD</b>	<b>outer diameter</b>
<b>OR</b>	<b>outer radius</b>
<b>ORNL</b>	<b>Oak Ridge National Laboratory</b>
<b>PCA</b>	<b>pool critical assembly</b>
<b>PWR</b>	<b>pressurized water reactor</b>
<b>RG</b>	<b>Regulatory Guide</b>
<b>RSICC</b>	<b>Radiation Safety Information Computational Center</b>
<b>T</b>	<b>vessel wall thickness</b>

## 8.0 References

---

1. Regulatory Guide 1.190, *Calculational and Dosimetry Methods for Determining Pressure Vessel Neutron Fluence*, U. S. Nuclear Regulatory Commission, March, 2001.
2. "Nine Mile Point Unit 1 Shroud Neutron Transport and Uncertainty Analysis", Report Number MPM-108679, MPM Technologies, Inc, 2161 Sandy Drive, State College, PA 16803-2283, October, 1998.
3. "Nine Mile Point Unit 2 Shroud Neutron Transport and Uncertainty Analysis", Report MPM-200623, MPM Technologies, Inc., 2161 Sandy Drive, State College, PA 16803-2283, February, 2000.
4. "Nine Mile Point Unit 2 3-Degree Pressure Vessel Surveillance Capsule Report", Report MPM-1200676, MPM Technologies, Inc., 2161 Sandy Drive, State College, PA 16803-2283, December, 2000.
5. "Nine Mile Point Unit 2 Shroud Neutron Transport and Uncertainty Analysis", Report MPM-301624, Revision 1, MPM Technologies, Inc., 2161 Sandy Drive, State College, PA 16803-2283, January, 2003.
6. "Nine Mile Point Unit 2 Shroud Neutron Transport and Uncertainty Analysis: Addendum", Report MPM-301624A, Revision 1 MPM Technologies, Inc., 2161 Sandy Drive, State College, PA 16803-2283, January, 2003.
7. Remec, I. and Kam, F.B.K., *Pool Critical Assembly Pressure Vessel Facility Benchmark*, NUREG/CR-6454, (ORNL/TM-13205), USNRC, July 1997.
8. Carew, J. F., Hu, K., Aronson, A., Prince, A., and Zamonsky, G., *PWR and BWR Pressure Vessel Fluence Calculational Benchmark Problems and Solutions*, NUREG/CR-6115 (BNL-NUREG-52395), Draft completed May 20, 1997.
9. RSICC Computer Code Collection, CCC-543, TORT-DORT-PC, Two- and Three-Dimensional Discrete Ordinates Transport Version 2.7.3, available from the Radiation Safety Information Computational Center, Oak Ridge National Laboratory, Oak Ridge, TN, June, 1996.
10. RSICC Data Library Collection, DLC-185, BUGLE-96, Coupled 47 Neutron, 20 Gamma Ray Group Cross Section Library Derived from ENDF/B-VI for LWR Shielding and Pressure Vessel Dosimetry Applications, available from the Radiation Safety Information Computational Center, Oak Ridge National Laboratory, Oak Ridge, TN, March, 1996.
11. RSICC Peripheral Shielding Routine Code Collection, PSR-277, LEPRICON, PWR Pressure Vessel Surveillance Dosimetry Analysis System, available from the Radiation Safety Information Computational Center, Oak Ridge National Laboratory, Oak Ridge, TN, June, 1995.

12. RSICC Computer Code Collection, CCC-371, "ORIGEN 2.1, Isotope Generation and Depletion Code Matrix Exponential Method," available from the Radiation Safety Information Computational Center, Oak Ridge National Laboratory, Oak Ridge, TN, May, 1999.
13. Fero, A.H., Anderson, S.L. and Roberts, G.K., "Analysis of the ORNL PCA Benchmark Using TORT and BUGLE-96," Reactor Dosimetry: Radiation Metrology and Assessment, ASTM STP 1398, John G. Williams, David W. Vehar, Frank H. Ruddy, and David Gilliam, Eds., American Society for Testing and Materials, West Conshohocken, PA, 2001.
14. Remec, I. and Kam, F.B.K., *H. B. Robinson-2 Pressure Vessel Benchmark*, NUREG/CR-6453 (ORNL/TM-13204), Oak Ridge National Laboratory, Oak Ridge, TN 37831, February, 1998.
15. ASTM Designation E482-01, *Standard Guide for Application of Neutron Transport Methods for Reactor Vessel Surveillance*, in ASTM Standards, Volume 12.02, American Society for Testing and Materials, Philadelphia, PA, 2002.
16. White, J. E., Ingersoll, D. T., Slater, C. O., Roussin, R. W., "BUGLE-96: A Revised Multigroup Cross Section Library for LWR Applications Based on ENDF/B-VI Release 3," (presented at the American Nuclear Society Radiation Protection & Shielding Topical Meeting, April 21-25, 1996, Falmouth, MA), April 1996.
17. Ingersoll, D. T., et. al., "Production and Testing of the VITAMIN-B6 Fine-Group and the BUGLE-93 Broad-Group Neutron/Photon Cross-Section Libraries Derived from ENDF/B-VI Nuclear Data," ORNL-6795, NUREG/CR-6214, January 1995.
18. Regulatory Guide 1.99, Revision 2, Radiation Embrittlement of Reactor Vessel Materials, U. S. Nuclear Regulatory Commission, May, 1988.
19. ASTM Designation E2006-99, *Standard Guide for Benchmark Testing of Light Water Reactor Calculations*, in ASTM Standards, Volume 12.02, American Society for Testing and Materials, Philadelphia, PA, 2002.
20. ASTM Designation E1018-01, *Standard Guide for Application of Neutron Transport Methods for Reactor Vessel Surveillance*, in ASTM Standards, Volume 12.02, American Society for Testing and Materials, Philadelphia, PA, 2002.
21. McElroy, W.N., Berg, S., Crockett, T., and Hawkins, R., "A Computer-Automated Iterative Method for Neutron Flux Spectral Determination by Foil Activation," AFWL-TR-67-41, Vol. I, 1967.
22. "International Reactor Dosimetry File (IRDF-90)," assembled by N. P. Kocherov and P. K. McLaughlin, IAEA-NDS-141 Rev. 2, October 1993.
23. Carew, J. F., private communication, June, 2001.
24. Letter SA-98-8, Anthony M. Salvagno (Constellation) to M.P. Manahan, "Data for NMP-1 Neutron Transport Analysis," February 10, 1998.
25. Letter, George B. Inch (Constellation) to M.P. Manahan, "Input Data for Core Best Estimate

- Fluence Calculations”, Aug. 7, 1998.
26. Letter FA98-32, Anthony M. Salvagno (Constellation) to M.P. Manahan, “Data for NMP-1 Neutron Transport Analysis-Final”, April 8, 1998.
  27. E-mail from J. Winklebleck (Constellation) to M. P. Manahan, Sr., “NMP-1 Fluence Data”, June 10, 2003.
  28. E-mail from J. Winklebleck (Constellation) to M. P. Manahan, Sr., “Problems with Fuels Data”, June 30, 2003.
  29. Federal Express Package, G. Inch (Constellation) to M. P. Manahan, “NMP-1 Information Needs”, Received at MPM 6/6/03.
  30. Federal Express Package, G. Inch (Constellation) to M. P. Manahan, “C5, 6, and 7 Summary Reports”, Received at MPM 6/9/03.
  31. E-mail from G. Inch (Constellation) to M. P. Manahan, Sr., “Data to be Used for Nine Mile Point Unit 1 BWR Transport Calculations”, Final Approval of Data Table, July 8, 2003.
  32. E-mail from G. Inch (Constellation) to M. P. Manahan, Sr., “Top Guide Details and Core Plate Details”, May 30, 2003.
  33. Fax from G. Inch (Constellation) to M. P. Manahan, Sr., “NMP-1 1973 Capsule Data”, May 30, 2003.
  34. E-mail from J. Winklebleck (Constellation) to M. P. Manahan, Sr., “In-Channel Void Fraction”, June 10, 2003.
  35. Letter from J. H. Morgan (General Electric) to T. J. Perkins (NMP-1), “Fast Fluence Determination at the Nine Mile Point Pressure Vessel,” October 14, 1974.
  36. Manahan, M. P., Failey, M. P., and Landow, M. P., “Final Report on Examination, Testing and Evaluation of the Nine Mile Point-Unit 1 30-Degree Azimuthal Surveillance Capsule,” BCL-587-P-4779, Battelle Columbus Laboratories, April 23, 1985.
  37. Stahl, D., et. al., “Final Report on Examination, Testing and Evaluation of Irradiated Pressure Vessel Surveillance Specimens from the Nine Mile Point Nuclear Power Station,” BCL-585-84-6, Battelle Columbus Laboratories, July 18, 1984.
  38. S. King, K. Hour, “Fluence Analysis Report for Boat Samples, Nine Mile Point 1”, January 29, 1998.
  39. Framatome Report 86-1266298-00, “Fluence Analysis Report for Boat Samples”, January, 1998.
  40. ASTM Designation E261-94, *Standard Practice for Determining Neutron Fluence, Fluence Rate, and Spectra by Radioactivation Techniques*, in ASTM Standards, Volume 12.02, American Society for Testing and Materials, Philadelphia, PA, 2002.
  41. Casmo-Simulate, Studsvik’s Advanced Three-Dimensional Two-Group Reactor Analhssi Code, Studsvik of America, Inc.

42. Ludwig, S. B. and Renier, J. P., "Standard- and Extended-Burnup PWR and BWR Reactor Models for the ORIGEN2 Computer Code," ORNL/TM-11018, December 1989.

## Appendix

### Application of ORIGEN Code for Determination of Fission Source by Isotope

Detailed data on the breakdown of fission by isotope was not available at the time the previous calculations were performed for NMP-1 and NMP-2. To overcome this deficiency, the ORIGEN (version 2.1) computer code [12] was used to calculate the fission distribution by isotope as a function of fuel burnup for use in the determination of the fission source. This application of the ORIGEN code was tested by comparisons of heavy element amounts with those from fuel depletion codes for other plants to verify that the ORIGEN output as a function of burnup is reasonable. In this appendix, comparisons of the transport results based on ORIGEN data with data from BWR fuel-specific calculations are reported to determine the magnitude of the difference. Constellation is currently using Studvik's Casmo-Simulate code [41] to provide core follow output, including isotopic data as a function of burnup.

ORIGEN uses a matrix exponential method to solve a large system of coupled, linear, first-order ordinary differential equations with constant coefficients in order to calculate the buildup, decay, and processing of radioactive materials. Supplied with the code are libraries for standard and extended burnup calculations [42]. Since ORIGEN uses a single cross section for each reaction at each time step, cross sections must be collapsed for the specific geometry being calculated. ORIGEN does vary cross sections with fuel burnup, but such effects as void fraction and other variables that can affect reaction rates are not taken into account. Comparisons with isotopic distributions from fuel depletion codes for burnup of BWR fuel in the typical ranges encountered in the outer fuel bundles in most BWR plants indicated that the best results were obtained with the BWR extended burnup library. This library was therefore selected for all BWR applications made to date.

Fuel encountered in BWR applications is initially uranium enriched to a few percent U235. As burnup occurs, U235 is removed and Pu239 is produced. Gradually more and more of the fission events occur in Pu239 and the higher plutonium isotopes. This has two effects on transport calculations. First, fissions in plutonium have a slightly more energetic fission spectrum, and thus a higher fraction of neutrons in the higher energy groups are produced. Differences in transport due to the change in spectrum will vary, depending on distance from the source. Second, both the neutrons per fission and the energy per fission increase with burnup, with the neutrons per fission increasing faster. Since the normalization of the transport calculation is proportional to the number of neutrons and inversely proportional to the energy per fission (since the calculation produces the neutron flux at a given reactor power), the high energy neutron flux increases with fuel burnup.

To validate the use of ORIGEN, NMP-1 cycle 9 was calculated using fission fractions determined both by Casmo-Simulate and by ORIGEN. For this case, the fuel in the outer two rows of bundles had an initial average enrichment of 2.77% and an average burnup in the outer rows of about 22000 MWd/MTU. The ORIGEN calculation resulted in a higher fraction of fissions in Pu for this burnup and thus the normalization of the transport runs for the ORIGEN

derived neutron source was higher by about 0.6%. Results for the two calculations are shown in Figure A-1 which presents the neutron flux above 1 MeV at the vessel inner radius at the maximum axial elevation. It is observed that the curves are in close agreement, with the ORIGEN source producing a calculated fluence rate that is uniformly higher by 1.3%. Thus the effect of the difference in neutron spectrum is about 0.7% when the 0.6% difference in normalization is subtracted.

The 1.3% difference may be compared with the estimated uncertainty in vessel fluence due to the spectrum and normalization uncertainty previously evaluated for NMP-1 in Reference [2]. This estimate was 2.9% for the vessel inner radius maximum fluence rate. Thus, the difference between ORIGEN and Casmo-Simulate sources falls well within the previously estimated uncertainty. Moreover, it should be noted that the ORIGEN result differs in a conservative direction, i.e. use of the ORIGEN data produce a higher calculated exposure.

Based on these results, it is concluded that the use of ORIGEN to determine the fraction of fissions from fuel isotopes is acceptable in lieu of using plant-specific data from fuel depletion codes. If ORIGEN is used, differences within the range of burnups considered are less than estimated uncertainties in results arising from the uncertainties in neutron spectrum and source normalization, and the error is in a conservative direction.

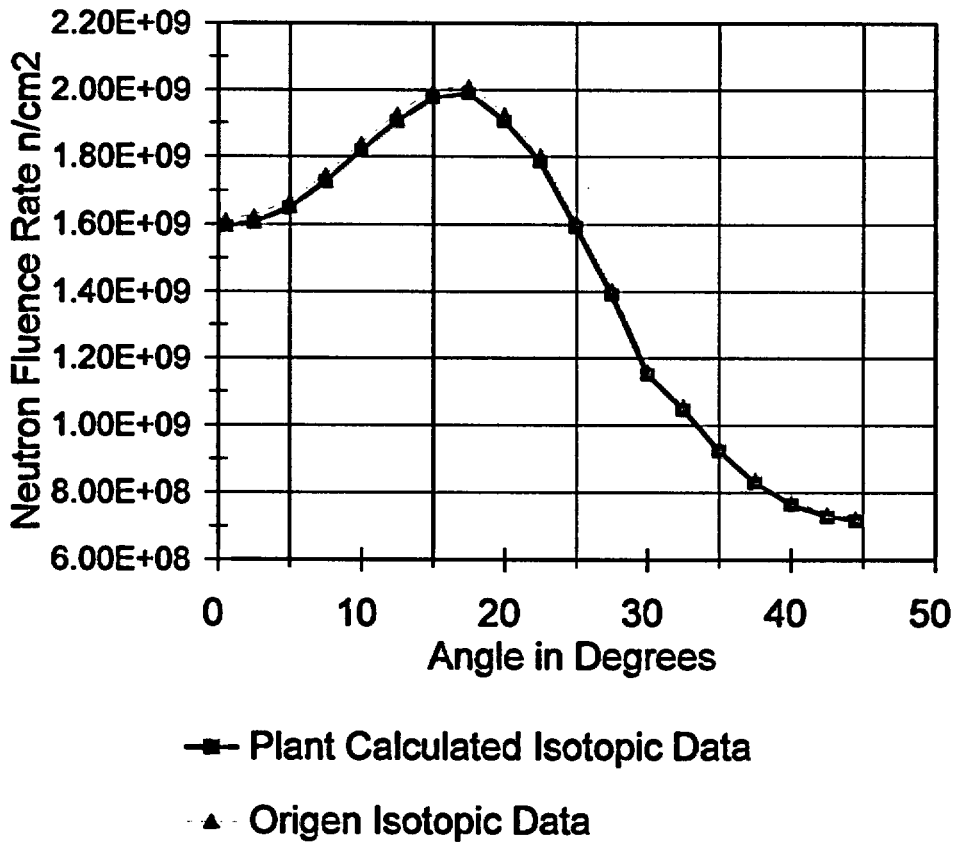


**Figure A-1** Average Fluence Rate for NMP-1 for Cycle 9 as a Function of Azimuthal Angle at the Maximum Axial Height Calculated Using Neutron Source Data from ORIGEN and from Casmo-Simulate.